

HPP-induced transcriptome response during recovery of *Listeria monocytogenes*

Ilhan Cem Duru (✉ ilhan.duru@helsinki.fi)

Institute of Biotechnology, University of Helsinki <https://orcid.org/0000-0003-3409-5215>

Florentina Ionela Bucur

Dunarea de Jos University of Galati Faculty of Sciences and Environment: Universitatea Dunarea de Jos din Galati
Facultatea de stiinte si Mediu

Margarita Andreevskaya

University of Helsinki: Helsingin Yliopisto

Bahareh Nikparvar

Norwegian University of Science and Technology: Norges teknisk-naturvitenskapelige universitet

Anne Ylinen

University of Helsinki: Helsingin Yliopisto

Leontina Grigore-Gurgu

Dunarea de Jos University of Galati Faculty of Sciences and Environment: Universitatea Dunarea de Jos din Galati
Facultatea de stiinte si Mediu

Tone Mari Rode

Norwegian Institute of Food Fisheries and Aquaculture Research: Nofima AS

Peter Crauwels

Ulm University: Universitat Ulm

Pia Laine

University of Helsinki: Helsingin Yliopisto

Lars Paulin

University of Helsinki: Helsingin Yliopisto

Trond Løvdal

Norwegian Institute of Food Fisheries and Aquaculture Research: Nofima AS

Christian U. Riedel

Ulm University: Universitat Ulm

Nadav Bar

Norwegian University of Science and Technology: Norges teknisk-naturvitenskapelige universitet

Daniela Borda

Dunarea de Jos University of Galati Faculty of Sciences and Environment: Universitatea Dunarea de Jos din Galati
Facultatea de stiinte si Mediu

Anca Ioana Nicolau

Dunarea de Jos University of Galati Faculty of Sciences and Environment: Universitatea Dunarea de Jos din Galati
Facultatea de stiinte si Mediu

Petri Auvinen

University of Helsinki: Helsingin Yliopisto

Research article

Keywords: HPP, *L. monocytogenes*, RO15, divIC, dicIVA, ftsE, ftsX

Posted Date: November 24th, 2020

DOI: <https://doi.org/10.21203/rs.3.rs-112830/v1>

License:  This work is licensed under a Creative Commons Attribution 4.0 International License. [Read Full License](#)

Version of Record: A version of this preprint was published at BMC Genomics on February 12th, 2021. See the published version at <https://doi.org/10.1186/s12864-021-07407-6>.

Abstract

Background

High-pressure processing (HPP) is a commonly used technique in the food industry to inactivate pathogens, including *L. monocytogenes*. It has been shown that *L. monocytogenes* is able to recover from HPP injuries and can start to grow again during long-term cold storage. To date, the gene expression profiling of *L. monocytogenes* during HPP damage recovery at cooling temperature has not been studied. In order to identify key genes that play a role in recovery of the damage caused by HPP treatment, we performed RNA-sequencing (RNA-seq) for two *L. monocytogenes* strains (barotolerant RO15 and barosensitive ScottA) at nine selected time points (up to 48 h) after treatment with two pressure levels (200 and 400 MPa).

Results

The results showed that a general stress response was activated by SigB after HPP treatment. In addition, the phosphotransferase system (PTS), protein folding, and cobalamin biosynthesis were the most upregulated genes during HPP damage recovery. We observed that cell-division-related genes (*divIC*, *dicIVA*, *ftsE*, and *ftsX*) were downregulated. By contrast, peptidoglycan-synthesis genes (*murG*, *murC*, and *pbp2A*) were upregulated. This indicates that cell-wall repair occurs as a part of HPP damage recovery. We also observed that prophage genes, including anti-CRISPR genes, were induced by HPP. Interestingly, a large amount of RNA-seq data (up to 85%) was mapped to Rli47, which is a non-coding RNA that is upregulated after HPP. Thus, we predicted that Rli47 plays a role in HPP damage recovery in *L. monocytogenes*. Moreover, gene-deletion experiments showed that amongst peptidoglycan biosynthesis genes, *pbp2A* mutants are more sensitive to HPP.

Conclusions

We identified several genes and mechanisms that may play a role in recovery from HPP damage of *L. monocytogenes*. Our study contributes to new information on pathogen inactivation by HPP.

Introduction

Listeria monocytogenes is a foodborne bacterial pathogen that poses a particular challenge to the food industry due to its ubiquitous nature and capability of adapting to various inhospitable environmental conditions related to food matrices and food processing environments [1, 2, 3]. Transmission of this bacterium to humans generally occurs *via* consumption of contaminated food, especially ready-to-eat (RTE) foods that do not undergo thermal treatment during the manufacturing process, such as RTE salads, dairy products from raw milk, vegetables, and fruits. Another food-product category of that sliced and packed meat products may be contaminated with *L. monocytogenes* is [4]. *L. monocytogenes* can cause listeriosis, a disease associated with a high number of hospitalization cases and mortality rates of 20–30% among people with weakened immune systems [4]. *L. monocytogenes* can resist a wide range of environmental conditions [5] and its ability to grow at refrigeration temperatures increases the risk of listeriosis [6].

The increasing demand of consumers for minimally processed foods, with fresh-like sensorial and nutritional properties, requires the implementation of alternative food processing techniques such as high-pressure processing (HPP). HPP is a relatively new, non-thermal processing technique that shows remarkable results with respect to pathogen inactivation and minimum impact on food quality [7, 8].

It has been reported that HPP causes morphological, structural, physiological, and genetic changes or damages to *L. monocytogenes* cells [9]. However, the susceptibility of *L. monocytogenes* to HPP varies between growth phase [10], strength of the cellular envelope [11], genomic features [12], and individual strains [13]. In addition, food matrix type, temperature, water activity, compression and decompression rates, applied pressure and holding time, and other extrinsic factors have an impact on inactivation of *L. monocytogenes* cells by HPP [9]. Several studies reported the potential of sublethally injured *L. monocytogenes* cells to recover after HPP and grow within the storage period even under refrigeration conditions [14, 15, 16, 17, 18]. Bozoglu et al. [19] showed that even though sublethally injured bacteria could not be detected immediately after HPP treatment of up to 550 MPa. However, injured but viable cells may be present in the pressurised samples as the authors detected growth after 6 days at 4 °C and already after 1 day at 22 °C and 30 °C.

Therefore, for an efficient decontamination process, the additional hurdles to increase efficiency of HPP and/or to prevent outgrowth of sublethally injured bacteria should be considered. In this context, it may be of interest to treat *L. monocytogenes* cells with antimicrobial agents that compromise cell wall and/or membrane and thereby render bacteria more sensitive to HPP and inhibit recovery. Such antimicrobial agents may include bacteriocins [20], essential oils [21, 22, 23], plant extracts [24], bacteriophages [25, 26], lysozyme [27, 28], lactoferrin [29], and lactoperoxidase [30].

Gene expression profiling of the response of *L. monocytogenes* to HPP has previously been studied by RNA-seq [12], microarray [31, 32], and qPCR [33]. For example, it has been shown that a mutation in *ctsR* causes barotolerance and a *ctsR* deletion mutant of *L. monocytogenes* shows increased expression of Clp protease and PTS system genes after HPP [31]. Similarly, we previously reported that heat-shock and Clp protease family genes were upregulated after HPP [12]. In contrast, Bowman et al. [32] reported downregulation of heat-shock and PTS system genes after HPP. The previous studies used relatively higher temperatures for storage after HPP (≥ 15 °C) compared to common cold-storage applications in the food industry. We recently showed genetic differences between barotolerant and barosensitive *L. monocytogenes* strains, which may explain their different HPP sensitivity [12]. Hence, in the present study, we investigate the transcriptional response to HPP and the differences in gene expression profiles between barotolerant and barosensitive *L. monocytogenes* strains during recovery. We selected *L. monocytogenes* strains RO15 (barotolerant) and ScottA (barosensitive) that were already analysed previously [12]. This is the first study to perform time-series RNA-seq using both barosensitive and barotolerant strains monitoring gene expression profiles during recovery of an HPP insult at 8 °C. We aimed to identify candidate genes that would be involved in the recovery of *L. monocytogenes* after HPP treatment.

Results

Log reduction testing of the strain RO15 and ScottA

We previously reported that strain RO15 is more resistant to treatment of 400 MPa for 1 minute compared to several other *L. monocytogenes* strains including strain ScottA [12]. Here, we sought to test the susceptibility of both strains to pressure treatment at 200 and 400 MPa for 8 minutes at 8 °C. While a treatment with 200 MPa was ineffective for inactivation of both strains, 400 MPa significantly reduced $\log_{10}(\text{cfu/ml})$ for both RO15 (5.78) and ScottA (7.04) compared to untreated samples ($p < 0.05$). The log reduction difference between the two strains was also statistically significant ($p < 0.05$; Fig. 1).

Differential Expression Analysis

After the HPP treatments, samples were taken at nine time points (0, 5, 10, 30, 45, 60 min and 6, 24, 48 h) and RNA-seq performed. Principal component analysis (PCA) of per gene read count data showed that there was a clear separation between HPP-treated samples and control samples for both 200 MPa and 400 MPa (Figure S1). In addition, we also saw clustering between early time points (0, 5, and 10 min), middle time points (30, 45, and 60 min), and late time points (6, 24, and 48 h) for 200 MPa treatment on a PCA plot (Figure S1).

Pairwise differential expression analysis between the treated samples and corresponding controls at all time points showed that a large number of genes were significantly differentially expressed (p -value ≤ 0.05) after HPP (Figure S2, Table S1, S2, S3, S4).

Differentially expressed genes and GO enrichment analysis

To gain a general perception of the functional groups of the differentially expressed genes, GO enrichment was performed (Fig. 2, Table S5). The most significantly enriched GO terms for upregulated genes were cobalamin biosynthetic process, divalent inorganic cation transport, and transition metal ion transport for both strains (Fig. 2). These GO terms were enriched at several time points in both strains after 200 and 400 MPa treatment. The main upregulated genes responsible for these GO terms enrichment were found in a large operon (OCPFDLNE_01234 - OCPFDLNE_01251 in the RO15 strain, LMOSA_20560 - LMOSA_20730 in the ScottA strain), including cobalamin biosynthesis genes, Cobalt ABC transporter, and Cobalt transport-related genes (Figure S3).

In *L. monocytogenes* RO15 HPP-upregulated genes were enriched at most time points in GO terms “phosphoenolpyruvate-dependent sugar phosphotransferase system (PTS system)” and “carbohydrate transmembrane transport” both after the 200 and 400 MPa treatment (Fig. 2, Table S5). In detail, upregulation was observed for the genes for fructose-, mannose-, galactitol-, cellobiose-, and ascorbate-specific PTS systems. Enrichment of these GO terms was also seen in the HPP-treated samples of *L. monocytogenes* ScottA strain taken, however, at later time points after HPP (both 200 and 400 MPa) (Fig. 2).

HPP caused upregulation of protein folding, chaperone, and peptidases genes, such as *clpE*, *clpP*, *groEL*, *groES*, *hrcA*, *dnaK*, and *dnaJ*, at 200 MPa at almost all time points and at 400 MPa at the early time points as reflected by an enrichment in the GO term “protein folding” (Fig. 2, 3c, 4c).

Significant downregulation was observed for cell division genes *divIC*, *dicIVA*, *ftsE*, and *ftsX* (Fig. 3i, 4i). In addition, in downregulated genes we observed a significant ($p < 0.05$) enrichment of the GO term “ATPase activity” (Table S5) at almost all timepoints for both pressure levels.

In addition to enriched GO terms, RNA-seq data was also analysed for specific gene families such as transcription factors (Fig. 3b and 4b, Figure S4) and transcription machinery genes (Fig. 3f and 4f, Figure S5). The gene *hrcA* (encoding heat-inducible transcription repressor HrcA) was upregulated at all time points for both RO15 and ScottA strains after 200 MPa, while after 400 MPa treatment upregulation was seen only in ScottA for the early time points (Fig. 3b, 4b). We also observed that gene *prfA* encoding the master regulator of virulence genes in *L. monocytogenes* was upregulated in both strains after both pressure treatments (Fig. 3b, 4b). Interestingly, only one of the *manR* genes encoding the transcriptional regulator ManR, which is found in two different copies in the genomes of ScottA and RO15, was upregulated in RO15 strain after HPP treatment but not in ScottA (Fig. 3b and 4b). With respect to the transcription machinery genes, *rpoD* encoding the RNA polymerase sigma factor RpoD was upregulated in both strains after HPP (Fig. 3f and 4f).

Upregulation of *nagA* (OCPFDLNE_01016) and two separate *nagB* genes (OCPFDLNE_01017 and OCPFDLNE_02454) was observed in RO15 at all timepoints. Similarly, ScottA showed upregulation of the *nagA* (LMOSA_18460) and

nagB (LMOSA_18470) homologues at early time points. However, the second *nagB* homologue of ScottA (LMOSA_3160) was not upregulated (Fig. 3a, 4a).

We also focused on mechanosensitive channel genes. The gene encoding a putative mechanosensitive channel gene of large conductance (*mscL*) was upregulated at early time points after 200 MPa treatment in RO15, while this upregulation was not seen in ScottA (Fig. 3h). After 400 MPa, both strains had similar *mscL* expression patterns with upregulation at late time points (Fig. 4h). The homologue for a mechanosensitive channel of small conductance (*ykuT*) was only upregulated in RO15 at 48 h after 200 MPa treatment (Fig. 3h).

To see the difference between the responses to the different pressure levels, we identified genes that were upregulated after 200 MPa treatment but not after 400 MPa and *vice versa* for each time point. In both strains, the genes that were upregulated after 200 MPa but not after 400 MPa at early time points were mainly related to translation (Table S6, Table S7). Interestingly, translation-related genes were upregulated after 400 MPa but not after 200 MPa in the RO15 on late time points (Table S6, Table S7). We observed upregulation of *hpf* gene (encoding ribosome hibernation promoting factor) in ScottA even at the time point 48 h (Fig. 4j). In addition, we also observed several cobalamin biosynthesis and PTS-related genes were upregulated at early time points after 400 MPa but not after 200 MPa in both strains (Table S6, Table S7).

Genes without orthologs within both strains were mainly phage genes and hypothetical genes. In both strains, phage genes were mostly upregulated after HPP (Figure S6, Figure S7). We previously reported that barotolerant strains harbour both CRISPR-Cas systems and anti-CRISPR genes [12]. However, upregulation of Cas genes was observed in neither of the two strains whereas anti-CRISPR genes (*acrIIA1* and *acrIIA2*) were significantly upregulated after HPP in RO15 (Figure S6).

Non-coding RNA (ncRNA)

RNA-seq read coverage plots showed that a very large amount of RNA-seq reads were mapped to non-coding regions, especially for RO15. Further examination showed that, on average, ~ 53% (ranging from 21–86%) of all RNA-seq reads for RO15 samples were mapped to the small non-coding RNA (ncRNA) *Rli47*. Similarly, ~ 28% (ranging from 6–72%) of the RNA-seq reads in samples of ScottA mapped to *Rli47* (Table S8, Table S9). Thus, we additionally performed expression analysis of ncRNAs. We observed that *Rli47* transcript levels were upregulated in response to pressure treatment in both strains (Figure S8). Similarly, levels of *LhrA* ncRNA were upregulated in both strains at the early timepoints. Interestingly, expression of *Rli53* was upregulated in RO15 after the pressure treatment, while no upregulation was seen in ScottA.

Gene regulatory networks based on RNA-seq data

One of our goals was to understand the regulatory networks involved in the response to HPP treatment in *L. monocytogenes* strains, RO15 and ScottA. Consensus gene network was created using the time-series expression data for all differentially expressed genes in both strains. This resulted in a total of 3661 gene network links (1506 genes and 3661 edges) for strain RO15 and 3427 gene network links (1389 genes and 3427 edges) for strain ScottA (Table S10). Interactive visualizations can be seen on https://icemduru.github.io/RO15_gene_network and https://icemduru.github.io/ScottA_gene_network. Moreover, we clustered the genes based on the network data (Table S10) using network clustering algorithm Map equation [34]. For RO15, 151 clusters were predicted in the gene network (Table S11), while for ScottA, 128 clusters were predicted (Table S12).

For both strains, heat shock and chaperone-related genes were clustered together (CI6 in RO15 and CI9 in ScottA, Fig. 5, 6). *De novo* motif discovery analysis resulted in a number of significant motifs (E-value < 0.05) for the

upstream regions of heat shock clusters (Cl6 in RO15 and Cl9 in ScottA), and one of the motif was significantly (E-value < 0.05) similar to the CtsR motif (Table S13, Table S14) from the PRODORIC database [35] in both strains. This indicates CtsR is a regulator for protein-folding genes in these strains. We also observed that *ctsR* was linked to heat-shock genes based on gene network inference (Table S11, Table S12). Notably, *nagA* and *nagB* are placed in the heat shock cluster (Cl9) in ScottA providing a hint that co-expression of protein folding genes and peptidoglycan biosynthesis genes after the pressure treatment was required together for recovery in ScottA. In addition, we observed that the heat-shock cluster (Cl9) in ScottA was linked to Cl4 (Fig. 6), which includes stress-related genes.

The prophage genes were highly interconnected in both strains; almost all genes of the three phages found in the same cluster in ScottA (Cl2, Fig. 6) indicate all three prophages show similar gene expression reactions in ScottA. Similarly, prophage 3 and prophage 5 genes were highly linked in RO15 (Cl2 and Cl3, Fig. 5). The prophage cluster (Cl2) was also linked to Cl4 (Fig. 6) in ScottA, which contains universal stress protein UspA genes (*uspA*), indicating that phage induction was connected to stress response in ScottA. The prophage cluster (Cl3) was linked to Cl5 in RO15 (Fig. 5), which includes *mscL*, i.e. the gene for a mechanosensitive channel gene of large conductance, and *cspA* encoding a cold-shock protein.

The genes of Cl9 in RO15 were enriched for The GO term “response to antibiotic”. This cluster also included genes *uspA* (for universal stress protein A), virulence factor *prfA* (the master regulator of virulence in *L. monocytogenes*), and *hpf* (ribosome hibernation promoting factor), which all were significantly upregulated in both strains after HPP treatment. A similar cluster containing *prfA* and *hpf* was seen in ScottA (Cl6). This implies that stress response, virulence and ribosome hibernation are linked to each other and co-occurred with HPP treatment in both strains. For ScottA, *de novo* motif discovery for the upstream region of Cl6 genes resulted in two significant motifs (E-value < 0.05; Table S14), one of them being significantly (E-value < 0.05) similar to SigB motif from PRODORIC database [35].

ddPCR for validation for RNA-seq Results

ddPCR was performed for the same ScottA samples that were used for RNA-seq to validate the differential expression results obtained using RNA-seq data. Nine genes were selected (Table S15) and three different time points were tested; 200 MPa time point 24 h (Fig. 7), 400 MPa time point 10 min (Figure S9) and 24 h (Figure S10). ddPCR results for 8 selected genes showed that the Pearson correlation was very strong (> 0.97) between ddPCR log₂ fold change and RNA-seq log₂ fold change results for all time points.

The influence of HPP on mutant strains` viability

Based on transcriptional analysis, we decided to perform additional experiments on HPP resistance with the mutants carrying deletions in selected candidate genes. These candidate genes were selected based on the gene-expression data and a potential role in barotolerance and recovery from HPP damage. The selected candidate genes were: *ykuT*, encoding a putative mechanosensitive ion channel of small conductance (OCPFDLNE_01076 and LMOSA_19040 in RO15 and ScottA); and *pbp2A*, encoding for the penicillin-binding protein A2 (OCPFDLNE_02389 and LMOSA_2530 in RO15 and ScottA). For both genes, deletion mutants were generated in the widely used *L. monocytogenes* model strain EGDe (*Imo1013* and *Imo2229* in EGDe, respectively). Successful deletion was validated by genome sequencing (Figure S11). In order to test the resistance of *Listeria monocytogenes* EGDe mutants to HPP, they were grown to stationary growth phase and subjected to HPP at 300 and 350 MPa with a holding time of 5 min. Susceptibility of the mutants to these treatments was assessed by detecting colony forming units. This revealed a reduction of ~ 5 log CFU/mL for Δ *Imo2229* cells and ~ 3 log CFU/mL for both Δ *Imo1013* and wild-type EGDe by the 350 MPa treatment and reduction of ~ 1 log CFU/mL for all three by 300 MPa treatment (Fig. 8). For both 300 MPa and 350 MPa

treatments, we observed a significant ($p < 0.05$) difference in colony forming units between wild-type and $\Delta lmo2229$. No significant difference was observed between wild-type and $\Delta lmo1013$.

Discussion

High pressure processing (HPP) is commonly used in the food industry to inactivate foodborne pathogens and spoilage microorganisms. However, it has been reported that *L. monocytogenes* is able to recover after HPP treatment during long-term storage [18, 19, 36]. To study gene expression response during early recovery of *L. monocytogenes* and identify genes that are important for recovery, we performed RNA-seq of samples taken at different time points after HPP at two different pressure levels (200 MPa and 400 MPa). To account for strain-dependent variation in the HPP response, experiments were performed with two strains: RO15, a strain that was shown to be more resistant to HPP than others; and ScottA, a strain that is more sensitive to HPP [12].

L. monocytogenes can recover within one day after injury caused by HPP for 10 min at 450 MPa and 45 °C [19]. Recovery of *L. monocytogenes* was also observed after six days of storage at 4 °C for injured bacteria following treatment with HPP at 550 MPa at 45 °C for 10 min [19]. Our results show that viability was unaffected in the two strains tested after HPP treatment at 200 MPa and 8 °C for 8 (Fig. 1), but a marked reduction in viable counts of several \log_{10} units was observed for both strains treated at 400 MPa. However, the reduction in viable counts was significantly higher in ScottA compared to RO15, which supports our previous observation that RO15 is more pressure tolerant [12].

The time-resolved RNA-seq data allowed us to perform gene-network analysis. To summarize the gene networks, we clustered genes assuming that genes within a cluster, and in linked clusters, are functionally related or interact during recovery from HPP [37, 38, 39]. HPP mainly affects expression of protein folding genes, PTS system genes, prophage genes, and cobalamin biosynthesis genes. We saw that in both strains, stress response genes, virulence genes, and ribosome hibernation promoting factor *hpf* gene were strongly linked to each other, indicating that during recovery from HPP, co-expression of these three factors was needed. It has also been reported that the general stress sigma factor B (σ^B) regulates *hpf*, *prfA* (encoding listeriolysin regulatory protein), and *UspA1,2* (encoding universal stress proteins A1 and A2) [40]. Environmental stress activates σ^B , which regulates more than 200 genes [40, 41]. In line with this, based on de novo motif discovery analysis, SigB transcription factor binding site-like motif was found in the upstream regions of the gene cluster (Cl6; Fig. 6, Table S14), which includes *prfA* and *hpf* in ScottA. This indicates that a general stress response was activated in *L. monocytogenes* by σ^B after HPP.

We have reported that a large portion (up to ~ 85%) of RNA-sequencing reads were mapped to Rli47 ncRNA, which was upregulated in both strains after pressure treatment. Similarly, previous studies have also reported that up to ~ 90% of all RNA-seq reads map to Rli47 ncRNA in *L. monocytogenes* [42, 43]. It has been shown that Rli47 plays a role in the response to acid stress [43] and oxidative stress [44]. In line with these observations, our data suggests that Rli47 is also involved in HPP recovery based on high expression level after HPP treatment. It has also been shown that Rli47 is regulated by σ^B [45]. This supports our observation of general stress response activation by σ^B after HPP. In addition, Rli53 expression was upregulated in RO15 but not in ScottA. Rli53 has been associated with antibiotic resistance [46]. Our results indicate that Rli53 may also play a role in pressure resistance in RO15.

Cobalamin biosynthesis was the most significantly enriched GO term for upregulated genes in both strains. It has been shown that cobalamin plays a protective role against oxidative stress in bacteria [47]. Cobalamin was also shown to be an essential cofactor for propanediol and ethanolamine utilization [48]. Significant downregulation of cobalamin biosynthesis genes in *L. monocytogenes* has been reported in response to Rli47 deletion [45]. Hence,

upregulated cobalamin synthesis genes after HPP in this study can be related to increased levels of Rli47, which is regulated by σ^B . We therefore predicted that cobalamin biosynthesis genes were upregulated as part of the general stress response of HPP.

Stress conditions have been shown to induce prophages in *L. monocytogenes* [49, 50]. Upregulation of prophage genes in both strains after HPP indicates that pressure stress also induces prophages. In addition, co-regulation of different prophages within the same host has also been shown in *L. monocytogenes* [50]. Similarly, our gene-network inference suggests that prophages were linked to each other within strains, coexpression of prophages genes were observed. Based on pan-genome analysis, we previously proposed that prophages and anti-CRISPR genes may play a role in pressure resistance in *L. monocytogenes* [12]. In this study we observed that both anti-CRISPR genes (*acrIIA1* (OCPFDLNE_02770, OCPFDLNE_02583) and *acrIIA2* (OCPFDLNE_02582)) in RO15 were upregulated after HPP.

GO enrichment analysis of upregulated genes indicated that PTS systems were activated in both strains for most of the time points during the recovery phase. Upregulation of PTS genes has also been reported for other stress conditions in *L. monocytogenes* based on transcriptome analysis [51, 52]. Upregulated PTS systems were mostly galactitol-, fructose-, and mannose-specific PTS systems. These carbon sources play a role in cell-wall biosynthesis [53, 54]. Thus, upregulation of these sugar transporters may be an indication of increased uptake of these sugars for cell-wall biosynthesis and as a carbon source to allow recovery from injury caused by HPP.

CtsR is a negative regulator of heat-shock genes, mainly of the *clp* family of genes, and has been shown to be directly involved in barotolerance of *L. monocytogenes* [55, 56, 57, 58, 59]. Deletion of *ctsR* led to an increase in barotolerance of ScottA by 5 orders of magnitude [58]. In addition, upregulation of PTS, heat-shock, and *clp* family genes has been reported for a ScottA *ctsR* mutant [31]. Furthermore, *ctsR* is reportedly regulated by σ^B in *Bacillus subtilis* [41]. Our results show upregulation of *ctsR* expression in both strains at some time points after treatment with 200 MPa but not with 400 MPa. Moreover, upregulation of genes was observed for heat-shock proteins of the *clp* family and chaperones in samples treated at both 200 MPa and 400 MPa in both strains (Fig. 3c, 4c). Especially *clpE* was one of the most significantly upregulated genes at several time points. It has been shown that heat-shock proteins are needed to deal with misfolded proteins, prevent cellular damage, and help cell recovery during pressure treatment [60]. Our observation that genes for heat-shock proteins are upregulated indicates a similar role in protection and recovery of *L. monocytogenes* to/after HPP treatment.

It has been shown that antibiotic resistant *L. monocytogenes* strains are more resistant to 400 MPa pressure treatment compared to antibiotic-susceptible strains [13]. Our previous pan-genome study [12] also showed that barotolerant strains have slightly different amino acid sequences for *norB* encoding a protein involved in resistance against quinolones. Interestingly, different strains showed variations in their expression of *norB*. Significant upregulation of *norB* was observed in barotolerant RO15 at several time points after 400 MPa treatment, including early time points. However, *norB* was only upregulated at the 24 h time point after 400 MPa treatment in barosensitive ScottA. This supports the observation that differences in antibiotic resistance genes might provide a different barotolerance level within *L. monocytogenes* strains.

Ribosome damage can lead to cell death after HPP [61]. Ribosome hibernation, that is dimerisation of 70S ribosomes leading to translationally inactive 100S particles, has been reported to occur as *L. monocytogenes* adapts to different stress conditions [62]. Ribosome hibernation involves the gene product of *hpf* (ribosome hibernation promoting factor) and upregulation of *hpf* was seen in both strains. Downregulation of *hpf* was observed at the 48 h time point after 200 MPa treatment only in RO15. In addition, in RO15, the GO term “translation” was also mainly enriched for upregulated genes at the late time points in RO15 at both 200 and 400 MPa (Fig. 2). However, no enrichment of GO

term “translation” was observed for upregulated genes in ScottA at 400 MPa (Fig. 2). Collectively, this indicates that *L. monocytogenes* keeps the translation inactive by inducing Hpf-mediated ribosome hibernation for a certain time after HPP. Moreover, there are differences between the strains in how long this hibernation lasts. The barotolerant strain RO15 seems to reactivate translation faster than the sensitive strain ScottA.

Based on morphological and physiological characterization, the cellular wall or membrane are targets to improve efficacy of HPP to inactivate *L. monocytogenes* [11]. We observed that peptidoglycan-synthesis genes such as, *murG*, *murC*, *murD*, and *pbp2A* were upregulated in both strains after HPP. Upregulation of peptidoglycan-synthesis genes with simultaneous downregulation of cell-division genes indicates that an active cell-wall repair occurs in both strains after HPP. *pbp2A* encodes a penicillin-binding protein that was shown to contribute to β -lactam resistance and cell morphology in *L. monocytogenes* [63]. To further investigate the role of this gene in response to HPP, a mutant carrying a deletion of the corresponding gene (*Imo2229*) was generated in *L. monocytogenes* strain EGDe and tested for resistance against HPP. The results show that the *Imo2229* mutant was significantly more sensitive to HPP than the parental wildtype strain (Fig. 8). This shows that *pbp2A* is an important factor in *L. monocytogenes* for recovery after HPP.

Peptidoglycan of bacteria consists of a backbone of alternating N-acetylglucosamine (GlcNAc) and N-acetylmuramic acid (MurNAc) units interconnected with peptide side-chains [64]. It has been shown that bacteria are able to recycle N-Acetylglucosamine from peptidoglycan using the proteins encoded by *nagA* and *nagB* [53, 65]. The genomes of *L. monocytogenes* RO15 and ScottA each contain two copies of *nagA* and *nagB*, respectively, and one of the copies of each *nagA* and *nagB* are organized in an operon. Expression of these *nagAB* copies were upregulated in both strains after HPP at 200 and 400 MPa. The second copy of *nagA* was not differentially expressed in either strains. Interestingly, the second copy of *nagB* gene (OCPFDLNE_02454) was only upregulated in RO15. This difference might partly explain the barotolerance difference between strains. Increasing protein levels of the NagB are associated with increased growth rate in *E. coli* [66]. Thus, more efficient biosynthesis of cell-wall peptidoglycans due to higher *NagB* levels may contribute to the higher barotolerance of RO15.

HPP creates a mechanical force that may result in deformation of the membrane. Mechanosensitive channels were shown to respond to membrane stress and help bacteria to cope with this stress [67]. We were intrigued by the observation that the *mscL* gene encoding a MS channel protein of large conductance was upregulated after 400 MPa pressure treatment in both strains. In addition, *ykuT* (encoding small MS channel protein) was upregulated at the 200 MPa 48 h time-point in RO15. However, the obtained *Imo1013* mutant showed no significant difference in susceptibility/resistance to HPP indicating that the small MS channel protein was not directly involved in pressure resistance or only has a minor effect.

Gene expression profiling under pressure treatment in *Listeria* was studied previously by Bowman et al. [32] using *L. monocytogenes* strain S2542. Notably, a significant negative correlation was observed for \log_2 FC results between the study by Bowman et al. [32] and our study. Our RNA-seq results were validated using ddPCR (Fig. 7) and they are consistent for two different strains under different pressure levels and several time points. We speculate that discordance between the results could potentially arise from different growth conditions or different methods for measuring gene-expression levels.

Overall, these findings may lead to new approaches to improve HPP efficacy. For example, we observed that the mannose phosphotransferase system (Man-PTS) was upregulated after HPP treatment. Man-PTS is the receptor for class IIa bacteriocins, such as pediocin or garvicin [68, 69, 70]. Thus, increased expression of these receptors may provide an opportunity to pre-treat food with IIa bacteriocins, which may increase susceptibility to HPP. However, *dltD*

upregulation in RO15 may lead to incorporation of more alanine residues [71], which increases the positive charge and consequently reduces affinity to cationic antimicrobials and bacteriocins. Interestingly, *dltD* was downregulated in ScottA indicating pre-treatment might be more effective for barosensitive strains. In addition, among peptidoglycan biosynthesis genes, deletion of *pbp2A* causes significant susceptibility to HPP. Hence new approaches could be sought by using peptidoglycan cross-linking.

Conclusion

Recovery and outgrowth of *L. monocytogenes* in food after HPP treatment is a serious problem for the food industry. The mechanism of recovery of *L. monocytogenes* after HPP has not been studied by genome-wide transcriptional profiling. Understanding how bacteria recover from HPP injury may help the food industry to develop new strategies for better inactivation of food pathogens. Here we reported a very detailed gene expression response of *L. monocytogenes* during recovery from HPP treatment using two strains (barotolerant and barosensitive), several time points, and two different pressure levels. Protein folding, PTS system, universal stress response, and cobalamin biosynthesis were the main activated functions in response to HPP treatment in *L. monocytogenes*. We showed that ncRNAs may also play a role in HPP injury recovery. Based on our results, several genes involved in barotolerance and recovery from HPP injury were predicted. Deletion of *pbp2A* suggests that it plays a role in barotolerance of *L. monocytogenes*. Further reverse-genetics experiments are required to validate our predictions based on RNA-seq.

Methods

High pressure processing for inactivation of strain RO15 and ScottA

Pressure treatment testing the log reduction was carried out using the QFP 2 L-700 (Avure Technologies Inc., Columbus, USA) as previously described [12], except that a holding time of 8 min, vessel water temp of 8 °C, and pressures of 200 and 400 MPa were used for strain RO15 (isolated as described previously [12]) and ScottA (CIP103575, obtained from Centre de Ressources Biologiques de l'Institut Pasteur, Paris, France). Immediately after pressure treatment, pressurized and untreated samples were serially ten-fold diluted in tryptic soy broth with 0.6% yeast extract (TSBYE; Oxoid, Basingstoke, Hampshire, England) and plated in triplicate on tryptic soy agar with 0.6% yeast extract (TSAYE; Oxoid, Basingstoke, Hampshire, England) by using a spiral plater (Eddy Jet; IUL Instruments, Barcelona, Spain). Pressurized samples at 400 MPa were additionally plated manually (100 μ L) without being diluted. TSAYE plates were incubated at 37 °C for 48 h prior to counting the colonies and estimating bacterial inactivation.

High pressure processing for RNA-seq

Volumes of 350 mL BHI broth (Oxoid, Basingstoke Hampshire, England) were inoculated with *L. monocytogenes* RO15, and Scott A (CIP103575, obtained from Centre de Ressources Biologiques de l'Institut Pasteur, Paris, France) strain, respectively, previously sub-cultured in the same growth medium at 37 °C, at an OD₆₀₀ value of ~ 0.1. The cultures were grown at 37 °C to early stationary phase (~ 1.3 OD₆₀₀), fully transferred into 2 mL tubes, and cooled by keeping them at 4 °C for 1 h. The samples were treated at 200 and 400 MPa, 8 °C, for 8 min, in multi-vessel high-pressure equipment (Resato, Roden, the Netherlands), using a mixture of water and propylene glycol as transmitting fluid (TR15, Resato). Due to adiabatic heating, liquid temperatures inside the vessel after pressure build-up had risen up to 16 °C after the 200 MPa treatment, and up to 23 °C after the 400 MPa treatment. The compression rate during pressure build up was 100 MPa/min and an extra 1 min was considered as equilibration time. The decompression of

the vessels took approximately 5 s. After HPP, the samples were maintained at 8 °C for certain times, considered as recovery time points, as follows: 0 min (T1), 5 min (T2), 10 min (T3), 30 min (T4), 45 min (T5), 60 min (T6), 6 h (T7), 24 h (T8), and 48 h (T9). Control samples were held at 8 °C at atmospheric pressure (Figure S12). At each time point, in order to stabilize the RNA, both treated samples (5 replicates) and corresponding controls (4 replicates) were transferred in 4 mL of RNA protect reagent (Qiagen, Hilden, Germany), incubated at room temperature for 5 min, pelleted by centrifugation at 5000 rpm and stored at -80 °C, until RNA was extracted.

RNA extraction

RNA was extracted from samples obtained from the barotolerance experiment (n = 320) with NucleoSpin RNA kit (Macherey-Nagel, Düren, Germany) as described previously [12].

RNA-sequencing

RNA-sequencing was performed for 216 samples from the barotolerance experiment including three replicate samples for each treatment and time point (Table S16). Prior to RNA-seq library preparation, rRNAs were removed by hybridizing extracted RNA with DNA oligos complementary to 16S, 23S, and 5S rRNAs followed by digestion of resulting DNA-RNA hybrid molecules. Hybridization reactions included 1 µg RNA, 1 x buffer (16.7 mM Tris-HCl, pH8, 33.3 mM KCl), and 250 nM pooled DNA oligos in a total volume of 12 µl. Reactions were incubated at 95 °C for 2 min, slowly (0.1 °C/sec) cooled to 22 °C, incubated at 22 °C for a further 5 min, and placed on ice. For digestion of rRNAs, 1.5 µl of 10 x RNaseH buffer, 0.2 µl RNaseH (Thermo Scientific, Waltham, Massachusetts, United States), 0.5 µl Ribolock RNase inhibitor (Thermo Scientific), and 0.8 µl of water were added. Digestion reactions were incubated at 37 °C for 60 min, and inactivated at 65 °C for 20 min. Remaining unhybridized DNA oligos were removed with RapidOut DNA Removal kit (Thermo Scientific) according to manufacturer's instructions. RNA-seq libraries were prepared using QIAseq stranded Total RNA Lib kit (Qiagen) using 1 reaction volumes. Due to the large number of samples, purification steps were performed with a Magnatrix1200 pipetting robot (Magnetic Biosolutions) using precipitation on Dynabeads MyOne Carboxylic acid beads (Invitrogen, Carlsbad, California, United States), and 10% PEG after reverse transcriptase and second strand synthesis steps, and 9.5% PEG after the strand-specific ligation step. Instead of the kit's adapter, a truncated TruSeq adapter was used in the strand-specific ligation. Libraries were amplified using half of the purified ligation product (10 µl) in 1 x HF buffer with 0.2 mM dNTPs, 0.6 µM dual-index primer [72], and one unit of Phusion Hot Start II High-Fidelity DNA polymerase (Thermo Fisher Scientific) in a total volume of 50 µl. The PCR protocol that was used was 98 °C, 30 s; 20 × (98 °C, 10 s; 65 °C, 30 s; 72 °C, 10 s); 72 °C, 5 min. Concentrations of amplified libraries were measured with a Qubit fluorometer and dsDNA HS assay kit (Invitrogen, Carlsbad, California, United States), and size distributions visualized with Fragment Analyzer and High Sensitivity NGS Fragment Analysis kit (Advanced Analytical, Parkersburg, WV, USA). Amplified libraries were pooled into two batches, each including 108 samples. The first pool was concentrated using an Amicon Ultra 100K column (Millipore, Burlington, MA, USA), purified once with 0.9 x AMPure XP beads (Beckman Coulter, Brea, CA, USA), and once with PEG (8–8.5%)/NaCl precipitation on Dynabeads MyOne™ carboxylic beads (Invitrogen). The second pool was purified twice with 0.9 x AMPure XP beads (Beckman Coulter). For both pools, size selection of 300–600 bp fragments was performed using BluePippin and 2% agarose gel cassette (Sage Science). Finally, the pools were purified with S-400 Microspin HR columns (GE Healthcare, Chicago, Illinois, United States). NextSeq 500 (Illumina, San Diego, CA, USA) was used to sequence the RNA-seq libraries twice. Altogether, seven sequencing runs were performed to produce 76 bp single-end reads.

RNA-seq data pre-processing and differential expression analysis.

RNA-seq reads obtained from all samples were processed using Trimmomatic v0.36 [73] to trim off the low-quality bases and filter out the adapter sequences. SortmeRNA v2.1b [74] was used to filter out ribosomal RNA reads. Reads were then mapped against the corresponding genomes (ScottA: GCA_000212455.1, R015: GCA_902827145.1) using bowtie2 v2.3.4.3 [75] with default settings. Counting of reads per gene was performed using HTSeq v0.9.1 [76] with union mode. Hierarchical clustering of samples (HCA) based on Euclidean distances and principal-component analysis (PCA) of the samples was done for each *L. monocytogenes* strain as described in the manual for the DESeq2 R package v1.22.2 [77] on “regularized log” (rlog)-transformed read count data to visually explore sample relationships. One sample in ScottA (R_046) and two samples in R015 (R_045, R_055) belonged neither to control nor to HPP clusters and were thus discarded as potential outliers. In addition, two R015 samples (R_057, R_235) contained a very low number of CDS-mapped reads (approx. 0.05 million) and were also discarded (Table S17).

Differential expression analysis for each *L. monocytogenes* strain was performed using R package DESeq2 v1.22.2 [77]. The comparisons were made in multiple ways: 1) Comparing the HPP-treated samples to the corresponding controls for each time point and at different HPP level, separately; 2) Comparing the time dynamics of gene expression (as described in DESeq2 manual, <http://master.bioconductor.org/packages/release/workflows/vignettes/rnaseqGene/inst/doc/rnaseqGene.html#time-course-experiments>) between control and treated samples, separately for 200 and 400 MPa series, to find the genes that changed expression at least at one time point; the gene expression at time point 0 in control was taken as a proxy for gene expression before the HPP treatment (designated as T00). Genes were considered to be significantly differentially expressed if their adjusted p-value ≤ 0.05 and their \log_2 fold change (\log_2 FC) ≥ 0.6 , (therefore, fold change FC ≥ 1.5). For the time dynamic comparison, genes were considered to be significantly differentially expressed at least at one time point if the adjusted p-value ≤ 0.05 .

Gene regulatory network construction, clustering and visualization

The initial set of genes used to build the network contained 1,964 genes for strain R015 and 1,852 genes for ScottA that changed expression between the corresponding controls and treatments at least at one time point (adjusted p-value < 0.05). The gene expression values used to build a network were regularized log (rlog) transformed as described in DESeq2 [77] to stabilize the variance and normalize the count data. Eleven networks have been built using 11 publicly available algorithms (clr, genie3, aracne, pearson_corr, narromi, pcor, plsnet, tigress, llr-ensemble, el-ensemble) embedded into Seidr toolkit [78] and integrated into one network using Seidr. The hard threshold for the edge score was manually chosen to be 0.4 based on the criteria described here (<https://seidr.readthedocs.io/en/latest/source/threshold/threshold.html>) leaving only 1,506 genes, 3,661 edges for strain R015, and 1,389 genes, 3,427 edges for strain ScottA in the final weighted undirected network. Infomap v0.19.26 [34] two-level clustering with options “-bftree - 2 -flow-network -N 10000” was used to find clusters (modules) of genes in the network and the flow between the modules (the strength of interactions between the modules). The two-level representation was visualized using the map&alluvial generator (<http://www.mapequation.org/apps/MapGenerator.html>). The network was visualized and centrality metrics calculated for the nodes (e.g. Degree, Betweenness and Closeness) using Cytoscape [79].

MEME suite v5.0.5 [80] was used for motif analysis. The upstream regions of genes ranging from 50 to 300 nucleotides were extracted using python script (https://github.com/peterthorpe5/intergenic_regions). *De novo* motif discovery was performed using MEME [80]. The discovered motifs were searched against transcription-factor binding-site databases, such as CollecTF [81], PRODORIC [35], RegTransBase [82], RegPrecise [83], DPINTERACT [84], and Swiss Regulon [85], using Tomtom tool [86]. The listed databases were downloaded from the MEME suite as

meme database format, except RegPrecise. For RegPrecise, all transcription factor binding site motifs for *Listeriaceae* were downloaded and converted to the meme database using sites2meme script from the MEME suite v5.0.5 [80].

Functional enrichment analyses of the DE gene lists

GO terms of the genes have been predicted using PANNZER2 [87] with default parameters. The lists of DE genes obtained from the different comparisons and the network gene clusters were tested for the enrichment of GO terms (belonging to the Biological Process ontology) using topGO package [88]. Enrichment for GO terms was tested separately for up- and downregulated genes. The reference set included all the GO term-annotated genes in the genome. The functional categories were considered to be enriched if $p\text{-value} \leq 0.05$. KAAS (KEGG Automatic Annotation Server) [89] was also used to obtain KO (KEGG Orthology) assignments of genes.

ddPCR

ddPCR was used to verify RNA-seq results of the barotolerance experiment ($n = 18$). Three replicate samples of each treatment or strain and their corresponding control samples were always analysed. Expression levels of ten genes: *recG*, *fusA*, *clpE*, *hly*, *agrB*, *ftsE*, *mscL*, *pflA*, *dnaK*, and *murA*, were quantified from ScottA samples treated with 200 MPa and recovered for 24 h, or treated with 400 MPa and recovered for 10 min. Expression levels of seven genes: *recG*, *fusA*, *clpE*, *hly*, *agrB*, *ftsE*, and *mscL* were quantified using ScottA samples treated with 400 MPa and recovered for 24 h. Primers (Table S15) were designed using Primer3Plus [90] and manufactured by Integrated DNA Technologies. The protocol included gDNA removal and RT-PCR steps as described previously [91]. To be able to compare expression levels of different samples, expression of the target genes (cDNA copies/ μl) was normalized using concentrations of two stably expressed genes: *recG* and *fusA*. To help comparison to RNA-seq, the results were expressed as \log_2 (gene concentration in treated sample/gene concentration in control sample) values.

Deletion of Imo1013 and Imo2229 genes from *L. monocytogenes* EGDe genome

The bacterial strains and plasmids used in the present study are listed in Table 1. Culture media utilized for the cultivation of *E. coli* and *L. monocytogenes* were Luria-Bertani (LB) broth (Sigma Aldrich, St. Louis, Missouri, United States) and brain heart infusion (BHI) broth (Oxoid), respectively. *E. coli* EC10B chemically competent cells were prepared with the CaCl_2 method [92] and *L. monocytogenes* EGDe electrocompetent cells were obtained as described earlier [93]. The selective antibiotics and their concentrations were used as follows: kanamycin, 50 $\mu\text{g}/\text{mL}$ for *E. coli*; erythromycin, 250 $\mu\text{g}/\text{mL}$ for *E. coli* and 5 $\mu\text{g}/\text{mL}$ for *L. monocytogenes*; chloramphenicol, 7.5 $\mu\text{g}/\text{ml}$ for *L. monocytogenes*.

Table 1
Strains and plasmids used in this study.

Plasmids and strains	Characteristics	Source/Reference
Plasmids		
<i>pORI280</i>	RepA – gene replacement vector, constitutive <i>lacZ</i> , 5.3 kb, Em ^r	[94]
<i>pORI280ADΔImo1013</i>	<i>pORI280</i> containing 503-bp region on either side flanking <i>Imo1013</i> deletion <i>pORI280</i> including both upstream and downstream flanking regions (503 bp each) of <i>Imo1013</i> deletion	This study
<i>pORI280ADΔImo2229</i>	<i>pORI280</i> containing 503-bp region on either side flanking <i>Imo2229</i> deletion <i>pORI280</i> including both upstream and downstream flanking regions (503 bp each) of <i>Imo2229</i> deletion	This study
<i>pVE6007</i>	Temperature-sensitive helper plasmid that provides RepA in <i>trans</i> , Cm ^r	[95]
E. coli strains		
EC10B	DH10B derivative with Kan ^r and RepA integrated in the <i>glgB</i> gene	[93]
EC10B/ <i>pORI280ADΔImo1013</i>	E. coli EC10B with <i>pORI280ADΔImo1013</i>	This study
EC10B/ <i>pORI280ADΔImo2229</i>	E. coli EC10B with <i>pORI280ADΔImo2229</i>	This study
L. monocytogenes strains		
EGDe	Serotype 1/2a	[93, 96]
EGDeΔ <i>Imo1013</i>	EGDe with the entire <i>Imo1013</i> gene deleted	This study
EGDeΔ <i>Imo2229</i>	EGDe with the entire <i>Imo2229</i> gene deleted	This study

Two *L. monocytogenes* EGDe mutants were generated by chromosomal mutagenesis of *Imo1013* and *Imo2229* genes, based on the system composed of *pORI280AD* recombinant vector and *pVE6007* helper plasmid, following the protocol provided by Monk et al. [93].

The oligonucleotide primers used to amplify the flanking regions that shared 20 bp overlapping ends with *Pst*I linearized *pORI280* vector (Thermo Scientific) and 20 bp overlapping ends between them are presented in Table 2.

Table 2
Primers used in the amplification of AB and CD fragments from *L. monocytogenes* EGDe genomic DNA

Primers	Sequence 5'-3'	Amplimer obtained
<i>lmo1013_AB_fwd</i>	TCGAATTCGAAGCTTCTGCATAACACCAATAGTCGCCCT	Upstream flanking fragment (AB) of <i>lmo1013</i> coding region including the start codon (ATG)
<i>lmo1013_AB_rev</i>	AGCGAATTGGCGTCTTTTACATTTTTTGGTCCACATCCT	
<i>lmo1013_CD_fwd</i>	AGGATGTGGACCAAAAAATGTAAAAAGACGCCAATTCGCT	Downstream flanking fragment (CD) of the <i>lmo1013</i> coding region including the stop codon (TAA)
<i>lmo1013_CD_rev</i>	ATGACGTCGACGCGTCTGCATAGTGCAGTTATTACGATTG	
<i>lmo2229_AB_fwd</i>	TCGAATTCGAAGCTTCTGCATCAGGTGGCTCGATTGCAAA	Upstream flanking fragment (AB) of the <i>lmo2229</i> coding region including the start codon (ATG)
<i>lmo2229_AB_rev</i>	GTAAAATGTGCTTTTAATTACATGTAAGTCTCCTATCTTC	
<i>lmo2229_CD_fwd</i>	GAAGATAGGAGAGTTACATGTAATTAAGCACATTTTAC	Downstream flanking fragment (CD) of the <i>lmo2229</i> coding region including the stop codon (TAA)
<i>lmo2229_CD_rev</i>	ATGACGTCGACGCGTCTGCATTACCATCTAAAGTAATTT	

AB and CD fragments were generated by high-fidelity PCR amplification from *L. monocytogenes* EGDe genomic DNA isolated with Jena Bioscience kit (Jena, Germany) according to the manufacturer instructions. The reaction mixture (25 µL) was prepared in accordance with the indications of Phusion High-Fidelity DNA (Thermo Scientific) manufacturer, including 3% DMSO, 0.5 µM of each primer and 200 µM of each deoxynucleoside triphosphate. The PCR reaction conditions consisted of an initial denaturation step at 98 °C for 30 s followed by 30 cycles of 98 °C for 10 s, 60 °C for 30 s, and 72 °C for 30 s/kb and then a final extension at 72 °C for 5 min.

After gel extraction and purification (FavorPrep™ GEL/PCR Purification Kit, Favorgen), the gene deletion flanking fragments were ligated into the cut *pORI280* backbone by Gibson assembly (2X Gibson Assembly® Ultra Master Mix, Synthetic Genomics Inc) reaction (*pORI280AD*). Following chemically competent *E. coli* EC10B cells' transformation with the recombinant vector by heat shock, colony PCR was employed to screen for transformants. This was done by AD fragment amplification from the total DNA released from the heat treated cells (94 °C, 15 min.) with KAPA Taq DNA Polymerase (Sigma Aldrich) and primers pairs *lmo1013_AB_fwd* / *lmo1013_CD_rev* and *lmo2229_AB_fwd* / *lmo2229_CD_rev*.

Further, the electroporation of *L. monocytogenes* EGDe and the site-directed mutagenesis of *lmo1013* and *lmo2229* genes were performed according to the protocol of Monk et al. [93]. Gene deletion screening was performed by Colony PCR using the primers pairs AB_fwd/CD_rev to amplify the genomic region that encompasses both flanking fragments and gene of interest.

Gene deletion from *L. monocytogenes* EGDe genome was further confirmed by DNA sequencing. The same methods were used for genome sequencing and assembly of wild-type EGDe, Δ *lmo1013*, and Δ *lmo2229* as described previously [12]. In addition, the reads were mapped to reference *L. monocytogenes* EGDe genome and using Bowtie2 v2.3.4.3 [75] and visualized using IGV v2.4.19 [97] to focus on deletion regions.

Resistance of *L. monocytogenes* EGDe mutants to HPP

The *L. monocytogenes* EGDe strains were grown in TSB with 0.6% yeast extract (TSB-YE) to early stationary phase, prepared as described previously in High pressure processing for RNA-seq method and then subjected to HPP at 300 and 350 MPa, 8 °C, for 5 min. Due to adiabatic heating, water temperatures in the middle of the vessel at the end of pressure treatment had risen to 23.28 °C after the 300 MPa treatment, and 23.88 °C after the 350 MPa treatment. Lower pressures than those chosen in the recovery experiments were selected to demonstrate if increased susceptibility of the mutants to HPP was acquired. Both control and treated samples were serially diluted 1:10 in PBS, plated on TSA with 0.6% yeast extract (TSA-YE) and incubated at 37 °C for 48 h.

Abbreviations

non-coding RNA (ncRNA), coding sequence (CDS), colony forming units (cfu), high pressure processing (HPP), megapascals (MPa)

Declarations

Ethics approval and consent to participate

Not applicable

Consent for publication

Not applicable

Availability of data and material

All sequencing data have been deposited in the European Nucleotide Archive (ENA) under accession code PRJEB34771.

Competing interests

The authors declare that they have no competing interests.

Funding

This study was supported within the ERA-IB2 consortium “SafeFood” (ID: ERA-IB-16- 247 014) by grants from Academy of Finland to PA (311717, 307856), by a grant of the Executive Agency for Higher Education, Research, Development and Innovation Funding in Romania to AIN (International and European Cooperation–250 Subprogramme 3.2–Horizon 2020–ContractNo. 15/2017) and by the Research Council of Norway (RCN), grant number 263499. ICD was supported by the MBDP doctoral program. The funders had no role in study design, data collection and interpretation, or the decision to submit the work for publication.

Authors' contributions

PA, AIN, DB, TL, CUR, and NB conceived and designed the study. TMR, LG, TL, FIB, LGG, BN, AIN, and DB collected the samples and performed the pressure treatments and viable cell count. FIB, PC, and LGG performed gene deletion experiments. ICD, MA, and PL performed the bioinformatics analyses. AY performed RNA extraction, sequencing preparation, and ddPCR. LP organized NGS assays. PC extracted DNA. ICD, MA, and FIB drafted the manuscript. All authors have read, commented, and approved the final manuscript.

Acknowledgements

We want to thank Kirsi Lipponen, Eeva-Marja and Paula Collin for performing the NGS procedures for this project. We wish to acknowledge CSC – IT Center for Science, Finland, for computational resources. Karin Tranøy and Laila Budal (Nofima) are acknowledged for laboratory assistance. We thank University of Helsinki Language Services and Jennifer Rowland for English language revisions.

References

1. Gahan CGM, Hill C. *Listeria monocytogenes*: survival and adaptation in the gastrointestinal tract. *Front Cell Infect Microbiol.* 2014;4. doi:10.3389/fcimb.2014.00009.
2. NicAogáin K, O’Byrne CP. The Role of Stress and Stress Adaptations in Determining the Fate of the Bacterial Pathogen *Listeria monocytogenes* in the Food Chain. *Front Microbiol.* 2016;7. doi:10.3389/fmicb.2016.01865.
3. Bucur FI, Grigore-Gurgu L, Crauwels P, Riedel CU, Nicolau AI. Resistance of *Listeria monocytogenes* to Stress Conditions Encountered in Food and Food Processing Environments. *Front Microbiol.* 2018;9. doi:10.3389/fmicb.2018.02700.
4. EFSA Panel on Biological Hazards (BIOHAZ), Ricci A, Allende A, Bolton D, Chemaly M, Davies R, et al. *Listeria monocytogenes* contamination of ready-to-eat foods and the risk for human health in the EU. *EFSA J.* 2018;16:e05134.
5. Buchanan RL, Gorris LGM, Hayman MM, Jackson TC, Whiting RC. A review of *Listeria monocytogenes*: An update on outbreaks, virulence, dose-response, ecology, and risk assessments. *Food Control.* 2017;75:1–13.
6. Chan YC, Wiedmann M. Physiology and genetics of *Listeria monocytogenes* survival and growth at cold temperatures. *Crit Rev Food Sci Nutr.* 2009;49:237–53.
7. Muntean M-V, Marian O, Barbieru V, Cătuțescu GM, Ranta O, Drocas I, et al. High Pressure Processing in Food Industry – Characteristics and Applications. *Agriculture and Agricultural Science Procedia.* 2016;10:377–83.
8. Woldemariam HW, Emire SA. High Pressure Processing of Foods for Microbial and Mycotoxins Control: current trends and future prospects. *Cogent Food Agric.* 2019;5:1622184.
9. Ferreira M, Almeida A, Delgadillo I, Saraiva J, Cunha Â. Susceptibility of *Listeria monocytogenes* to high pressure processing: A review. *Food Reviews International.* 2016;32:377–99.
10. Wen J, Anantheswaran RC, Knabel SJ. Changes in barotolerance, thermotolerance, and cellular morphology throughout the life cycle of *Listeria monocytogenes*. *Appl Environ Microbiol.* 2009;75:1581–8.
11. Ritz M, Tholozan JL, Federighi M, Pilet MF. Morphological and physiological characterization of *Listeria monocytogenes* subjected to high hydrostatic pressure. *Appl Environ Microbiol.* 2001;67:2240–7.
12. Duru IC, Andreevskaya M, Laine P, Rode TM, Ylinen A, Løvdal T, et al. Genomic characterization of the most barotolerant *Listeria monocytogenes* RO15 strain compared to reference strains used to evaluate food high pressure processing. *BMC Genomics.* 2020;21:455.

13. Bruschi C, Komora N, Castro SM, Saraiva J, Ferreira VB, Teixeira P. High hydrostatic pressure effects on *Listeria monocytogenes* and *L. innocua*: Evidence for variability in inactivation behaviour and in resistance to pediocin bacHA-6111-2. *Food Microbiol.* 2017;64:226–31.
14. Koseki S, Mizuno Y, Yamamoto K. Predictive modelling of the recovery of *Listeria monocytogenes* on sliced cooked ham after high pressure processing. *Int J Food Microbiol.* 2007;119:300–7.
15. Koseki S, Mizuno Y, Yamamoto K. Use of mild-heat treatment following high-pressure processing to prevent recovery of pressure-injured *Listeria monocytogenes* in milk. *Food Microbiol.* 2008;25:288–93.
16. Tomasula PM, Renye JA, Van Hekken DL, Tunick MH, Kwoczak R, Toht M, et al. Effect of high-pressure processing on reduction of *Listeria monocytogenes* in packaged Queso Fresco. *J Dairy Sci.* 2014;97:1281–95.
17. Valdramidis VP, Patterson MF, Linton M. Modelling the recovery of *Listeria monocytogenes* in high pressure processed simulated cured meat. *Food Control.* 2015;47:353–8.
18. Nakaura Y, Morimatsu K, Inaoka T, Yamamoto K. *Listeria monocytogenes* cells injured by high hydrostatic pressure and their recovery in nutrient-rich or -free medium during cold storage. *High Press Res.* 2019;39:324–33.
19. Bozoglu F, Alpas H, Kaletunç G. Injury recovery of foodborne pathogens in high hydrostatic pressure treated milk during storage. *FEMS Immunol Med Microbiol.* 2004;40:243–7.
20. Liu G, Wang Y, Gui M, Zheng H, Dai R, Li P. Combined effect of high hydrostatic pressure and enterocin LM-2 on the refrigerated shelf life of ready-to-eat sliced vacuum-packed cooked ham. *Food Control.* 2012;24:64–71.
21. Evrendilek GA, Balasubramaniam VM. Inactivation of *Listeria monocytogenes* and *Listeria innocua* in yogurt drink applying combination of high pressure processing and mint essential oils. *Food Control.* 2011;22:1435–41.
22. Espina L, García-Gonzalo D, Laglaoui A, Mackey BM, Pagán R. Synergistic combinations of high hydrostatic pressure and essential oils or their constituents and their use in preservation of fruit juices. *Int J Food Microbiol.* 2013;161:23–30.
23. Stratakos ACh, Delgado-Pando G, Linton M, Patterson MF, Koidis A. Synergism between high-pressure processing and active packaging against *Listeria monocytogenes* in ready-to-eat chicken breast. *Innov Food Sci Emerg Technol.* 2015;27:41–7.
24. Bleoancă I, Saje K, Mihalcea L, Oniciuc E-A, Smole-Mozina S, Nicolau AI, et al. Contribution of high pressure and thyme extract to control *Listeria monocytogenes* in fresh cheese - A hurdle approach. *Innov Food Sci Emerg Technol.* 2016;38:7–14.
25. Komora N, Maciel C, Pinto CA, Ferreira V, Brandão TRS, Saraiva JMA, et al. Non-thermal approach to *Listeria monocytogenes* inactivation in milk: The combined effect of high pressure, pediocin PA-1 and bacteriophage P100. *Food Microbiol.* 2020;86:103315.
26. Komora N, Bruschi C, Ferreira V, Maciel C, Brandão TRS, Fernandes R, et al. The protective effect of food matrices on *Listeria lytic* bacteriophage P100 application towards high pressure processing. *Food Microbiol.* 2018;76:416–25.
27. Vannini L, Lanciotti R, Baldi D, Guerzoni ME. Interactions between high pressure homogenization and antimicrobial activity of lysozyme and lactoperoxidase. *Int J Food Microbiol.* 2004;94:123–35.
28. Iucci L, Patrignani F, Vallicelli M, Guerzoni ME, Lanciotti R. Effects of high pressure homogenization on the activity of lysozyme and lactoferrin against *Listeria monocytogenes*. *Food Control.* 2007;18:558–65.
29. Bravo D, de Alba M, Medina M. Combined treatments of high-pressure with the lactoperoxidase system or lactoferrin on the inactivation of *Listeria monocytogenes*, *Salmonella Enteritidis* and *Escherichia coli* O157:H7 in beef carpaccio. *Food Microbiol.* 2014;41:27–32.

30. Montiel R, Bravo D, de Alba M, Gaya P, Medina M. Combined effect of high pressure treatments and the lactoperoxidase system on the inactivation of *Listeria monocytogenes* in cold-smoked salmon. *Innov Food Sci Emerg Technol.* 2012;16:26–32.
31. Liu Y, Ream A, Joerger RD, Liu J, Wang Y. Gene expression profiling of a pressure-tolerant *Listeria monocytogenes* Scott A *ctsR* deletion mutant. *J Ind Microbiol Biotechnol.* 2011;38:1523–33.
32. Bowman JP, Bittencourt CR, Ross T. Differential gene expression of *Listeria monocytogenes* during high hydrostatic pressure processing. *Microbiology (Reading).* 2008;154 Pt 2:462–75.
33. Pérez-Baltar A, Alía A, Rodríguez A, Córdoba JJ, Medina M, Montiel R. Impact of Water Activity on the Inactivation and Gene Expression of *Listeria monocytogenes* during Refrigerated Storage of Pressurized Dry-Cured Ham. *Foods.* 2020;9.
34. Rosvall M, Axelsson D, Bergstrom CT. The map equation. *Eur Phys J Spec Top.* 2009;178:13–23.
35. Münch R, Hiller K, Barg H, Heldt D, Linz S, Wingender E, et al. PRODORIC: prokaryotic database of gene regulation. *Nucleic Acids Res.* 2003;31:266–9.
36. Bull MK, Hayman MM, Stewart CM, Szabo EA, Knabel SJ. Effect of prior growth temperature, type of enrichment medium, and temperature and time of storage on recovery of *Listeria monocytogenes* following high pressure processing of milk. *Int J Food Microbiol.* 2005;101:53–61.
37. Luo F, Yang Y, Zhong J, Gao H, Khan L, Thompson DK, et al. Constructing gene co-expression networks and predicting functions of unknown genes by random matrix theory. *BMC Bioinformatics.* 2007;8:299.
38. van Dam S, Vösa U, van der Graaf A, Franke L, de Magalhães JP. Gene co-expression analysis for functional classification and gene-disease predictions. *Brief Bioinformatics.* 2018;19:575–92.
39. Schlitt T, Palin K, Rung J, Dietmann S, Lappe M, Ukkonen E, et al. From gene networks to gene function. *Genome Res.* 2003;13:2568–76.
40. Liu Y, Orsi RH, Gaballa A, Wiedmann M, Boor KJ, Guariglia-Oropeza V. Systematic review of the *Listeria monocytogenes* σ B regulon supports a role in stress response, virulence and metabolism. *Future Microbiol.* 2019;14:801–28.
41. Bonilla CY. Generally Stressed Out Bacteria: Environmental Stress Response Mechanisms in Gram-Positive Bacteria. *Integr Comp Biol.* 2020;60:126–33.
42. Anast JM, Schmitz-Esser S. The transcriptome of *Listeria monocytogenes* during co-cultivation with cheese rind bacteria suggests adaptation by induction of ethanolamine and 1,2-propanediol catabolism pathway genes. *PLoS One.* 2020;15. doi:10.1371/journal.pone.0233945.
43. Cortes BW, Naditz AL, Anast JM, Schmitz-Esser S. Transcriptome Sequencing of *Listeria monocytogenes* Reveals Major Gene Expression Changes in Response to Lactic Acid Stress Exposure but a Less Pronounced Response to Oxidative Stress. *Front Microbiol.* 2020;10. doi:10.3389/fmicb.2019.03110.
44. Mujahid S, Bergholz TM, Oliver HF, Boor KJ, Wiedmann M. Exploration of the role of the non-coding RNA *SbrE* in *L. monocytogenes* stress response. *Int J Mol Sci.* 2012;14:378–93.
45. Marinho CM, Dos Santos PT, Kallipolitis BH, Johansson J, Ignatov D, Guerreiro DN, et al. The σ B-dependent regulatory sRNA *Rli47* represses isoleucine biosynthesis in *Listeria monocytogenes* through a direct interaction with the *ilvA* transcript. *RNA Biol.* 2019;16:1424–37.
46. Dar D, Shamir M, Mellin JR, Koutero M, Stern-Ginossar N, Cossart P, et al. Term-seq reveals abundant ribo-regulation of antibiotics resistance in bacteria. *Science.* 2016;352:aad9822.
47. Ferrer A, Rivera J, Zapata C, Norambuena J, Sandoval Á, Chávez R, et al. Cobalamin Protection against Oxidative Stress in the Acidophilic Iron-oxidizing Bacterium *Leptospirillum* Group II CF-1. *Front Microbiol.* 2016;7.

doi:10.3389/fmicb.2016.00748.

48. Mellin JR, Tiensuu T, Bécavin C, Gouin E, Johansson J, Cossart P. A riboswitch-regulated antisense RNA in *Listeria monocytogenes*. *Proc Natl Acad Sci U S A*. 2013;110:13132–7.
49. Ivy RA, Wiedmann M, Boor KJ. *Listeria monocytogenes* Grown at 7°C Shows Reduced Acid Survival and an Altered Transcriptional Response to Acid Shock Compared to *L. monocytogenes* Grown at 37°C. *Appl Environ Microbiol*. 2012;78:3824–36.
50. Argov T, Sapir SR, Pasechnek A, Azulay G, Stadnyuk O, Rabinovich L, et al. Coordination of cohabiting phage elements supports bacteria-phage cooperation. *Nat Commun*. 2019;10:5288.
51. Casey A, Fox EM, Schmitz-Esser S, Coffey A, McAuliffe O, Jordan K. Transcriptome analysis of *Listeria monocytogenes* exposed to biocide stress reveals a multi-system response involving cell wall synthesis, sugar uptake, and motility. *Front Microbiol*. 2014;5. doi:10.3389/fmicb.2014.00068.
52. Tang S, Orsi RH, den Bakker HC, Wiedmann M, Boor KJ, Bergholz TM. Transcriptomic Analysis of the Adaptation of *Listeria monocytogenes* to Growth on Vacuum-Packed Cold Smoked Salmon. *Appl Environ Microbiol*. 2015;81:6812–24.
53. Popowska M, Osińska M, Rzeczowska M. N-acetylglucosamine-6-phosphate deacetylase (NagA) of *Listeria monocytogenes* EGD, an essential enzyme for the metabolism and recycling of amino sugars. *Arch Microbiol*. 2012;194:255–68.
54. Vogler AP, Lengeler JW. Analysis of the nag regulon from *Escherichia coli* K12 and *Klebsiella pneumoniae* and of its regulation. *Mol Gen Genet*. 1989;219:97–105.
55. Karatzas KAG, Wouters JA, Gahan CGM, Hill C, Abee T, Bennik MHJ. The CtsR regulator of *Listeria monocytogenes* contains a variant glycine repeat region that affects piezotolerance, stress resistance, motility and virulence. *Mol Microbiol*. 2003;49:1227–38.
56. Karatzas KAG, Bennik MHJ. Characterization of a *Listeria monocytogenes* Scott A Isolate with High Tolerance towards High Hydrostatic Pressure. *Appl Environ Microbiol*. 2002;68:3183–9.
57. Karatzas KAG, Valdramidis VP, Wells-Bennik MHJ. Contingency Locus in *ctsR* of *Listeria monocytogenes* Scott A: a Strategy for Occurrence of Abundant Piezotolerant Isolates within Clonal Populations. *Appl Environ Microbiol*. 2005;71:8390–6.
58. Joerger RD, Chen H, Kniel KE. Characterization of a spontaneous, pressure-tolerant *Listeria monocytogenes* Scott A *ctsR* deletion mutant. *Foodborne Pathog Dis*. 2006;3:196–202.
59. Van Boeijen IKH, Chavarroche AAE, Valderrama WB, Moezelaar R, Zwietering MH, Abee T. Population Diversity of *Listeria monocytogenes* LO28: Phenotypic and Genotypic Characterization of Variants Resistant to High Hydrostatic Pressure. *Appl Environ Microbiol*. 2010;76:2225–33.
60. Aertsen A, Vanoirbeek K, De Spiegeleer P, Sermon J, Hauben K, Farewell A, et al. Heat Shock Protein-Mediated Resistance to High Hydrostatic Pressure in *Escherichia coli*. *Appl Environ Microbiol*. 2004;70:2660–6.
61. Niven GW, Miles CA, Mackey BM. The effects of hydrostatic pressure on ribosome conformation in *Escherichia coli*: and in vivo study using differential scanning calorimetry. *Microbiology (Reading)*. 1999;145 (Pt 2):419–25.
62. Kline BC, McKay SL, Tang WW, Portnoy DA. The *Listeria monocytogenes* hibernation-promoting factor is required for the formation of 100S ribosomes, optimal fitness, and pathogenesis. *J Bacteriol*. 2015;197:581–91.
63. Guinane CM, Cotter PD, Ross RP, Hill C. Contribution of Penicillin-Binding Protein Homologs to Antibiotic Resistance, Cell Morphology, and Virulence of *Listeria monocytogenes* EGDe. *Antimicrob Agents Chemother*. 2006;50:2824–8.

64. Vollmer W, Blanot D, de Pedro MA. Peptidoglycan structure and architecture. *FEMS Microbiol Rev.* 2008;32:149–67.
65. Park JT, Uehara T. How bacteria consume their own exoskeletons (turnover and recycling of cell wall peptidoglycan). *Microbiol Mol Biol Rev.* 2008;72:211–27, table of contents.
66. Alvarez-Añorve LI, Calcagno ML, Plumbridge J. Why does *Escherichia coli* grow more slowly on glucosamine than on N-acetylglucosamine? Effects of enzyme levels and allosteric activation of GlcN6P deaminase (NagB) on growth rates. *J Bacteriol.* 2005;187:2974–82.
67. Booth IR, Edwards MD, Black S, Schumann U, Miller S. Mechanosensitive channels in bacteria: signs of closure? *Nat Rev Microbiol.* 2007;5:431–40.
68. Tymoszewska A, Diep DB, Wirtek P, Aleksandrak-Piekarczyk T. The Non-Lantibiotic Bacteriocin Garvicin Q Targets Man-PTS in a Broad Spectrum of Sensitive Bacterial Genera. *Sci Rep.* 2017;7:8359.
69. Diep DB, Skaugen M, Salehian Z, Holo H, Nes IF. Common mechanisms of target cell recognition and immunity for class II bacteriocins. *Proc Natl Acad Sci U S A.* 2007;104:2384–9.
70. Ríos Colombo NS, Chalón MC, Navarro SA, Bellomio A. Pediocin-like bacteriocins: new perspectives on mechanism of action and immunity. *Curr Genet.* 2018;64:345–51.
71. Abachin E, Poyart C, Pellegrini E, Milohanic E, Fiedler F, Berche P, et al. Formation of D-alanyl-lipoteichoic acid is required for adhesion and virulence of *Listeria monocytogenes*. *Mol Microbiol.* 2002;43:1–14.
72. Somervuo P, Koskinen P, Mei P, Holm L, Auvinen P, Paulin L. BARCOSEL: a tool for selecting an optimal barcode set for high-throughput sequencing. *BMC Bioinformatics.* 2018;19:257.
73. Bolger AM, Lohse M, Usadel B. Trimmomatic: a flexible trimmer for Illumina sequence data. *Bioinformatics.* 2014;30:2114–20.
74. Kopylova E, Noé L, Touzet H. SortMeRNA: fast and accurate filtering of ribosomal RNAs in metatranscriptomic data. *Bioinformatics.* 2012;28:3211–7.
75. Langmead B, Salzberg SL. Fast gapped-read alignment with Bowtie 2. *Nat Methods.* 2012;9:357–9.
76. Anders S, Pyl PT, Huber W. HTSeq—a Python framework to work with high-throughput sequencing data. *Bioinformatics.* 2015;31:166–9.
77. Love MI, Huber W, Anders S. Moderated estimation of fold change and dispersion for RNA-seq data with DESeq2. *Genome Biol.* 2014;15:550.
78. Schiffthaler B, Serrano A, Street N, Delhomme N. Seidr: a gene meta-network calculation toolkit. *bioRxiv.* 2019;:250696.
79. Shannon P, Markiel A, Ozier O, Baliga NS, Wang JT, Ramage D, et al. Cytoscape: a software environment for integrated models of biomolecular interaction networks. *Genome Res.* 2003;13:2498–504.
80. Bailey TL, Boden M, Buske FA, Frith M, Grant CE, Clementi L, et al. MEME SUITE: tools for motif discovery and searching. *Nucleic Acids Res.* 2009;37 Web Server issue:W202-208.
81. Kiliç S, White ER, Sagitova DM, Cornish JP, Erill I. CollecTF: a database of experimentally validated transcription factor-binding sites in Bacteria. *Nucleic Acids Res.* 2014;42 Database issue:D156-160.
82. Cipriano MJ, Novichkov PN, Kazakov AE, Rodionov DA, Arkin AP, Gelfand MS, et al. RegTransBase—a database of regulatory sequences and interactions based on literature: a resource for investigating transcriptional regulation in prokaryotes. *BMC Genomics.* 2013;14:213.
83. Novichkov PS, Kazakov AE, Ravcheev DA, Leyn SA, Kovaleva GY, Sutormin RA, et al. RegPrecise 3.0—a resource for genome-scale exploration of transcriptional regulation in bacteria. *BMC Genomics.* 2013;14:745.

84. Robison K, McGuire AM, Church GM. A comprehensive library of DNA-binding site matrices for 55 proteins applied to the complete *Escherichia coli* K-12 genome. *J Mol Biol.* 1998;284:241–54.
85. Pachkov M, Balwiercz PJ, Arnold P, Ozonov E, van Nimwegen E. SwissRegulon, a database of genome-wide annotations of regulatory sites: recent updates. *Nucleic Acids Res.* 2013;41 Database issue:D214-220.
86. Gupta S, Stamatoyannopoulos JA, Bailey TL, Noble WS. Quantifying similarity between motifs. *Genome Biol.* 2007;8:R24.
87. Törönen P, Medlar A, Holm L. PANNZER2: a rapid functional annotation web server. *Nucleic Acids Res.* 2018;46:W84–8.
88. Alexa A, Rahnenfuhrer J. topGO: topGO: Enrichment analysis for Gene Ontology. Available at: <https://bioconductor.org/packages/release/bioc/html/topGO.html>
89. Moriya Y, Itoh M, Okuda S, Yoshizawa AC, Kanehisa M. KAAS: an automatic genome annotation and pathway reconstruction server. *Nucleic Acids Res.* 2007;35 Web Server issue:W182-185.
90. Untergasser A, Nijveen H, Rao X, Bisseling T, Geurts R, Leunissen JAM. Primer3Plus, an enhanced web interface to Primer3. *Nucleic Acids Res.* 2007;35 Web Server issue:W71-74.
91. Andreevskaya M, Jääskeläinen E, Johansson P, Ylinen A, Paulin L, Björkroth J, et al. Food Spoilage-Associated *Leuconostoc*, *Lactococcus*, and *Lactobacillus* Species Display Different Survival Strategies in Response to Competition. *Appl Environ Microbiol.* 2018;84.
92. Chang AY, Chau VWY, Landas JA, Pang Y. Preparation of calcium competent *Escherichia coli* and heat-shock transformation. *The Undergraduate Journal of Experimental Microbiology and Immunology.* 2017;1, 22-25.
93. Monk IR, Gahan CGM, Hill C. Tools for Functional Postgenomic Analysis of *Listeria monocytogenes*. *Appl Environ Microbiol.* 2008;74:3921–34.
94. Leenhouts K, Buist G, Bolhuis A, ten Berge A, Kiel J, Mierau I, et al. A general system for generating unlabelled gene replacements in bacterial chromosomes. *Mol Gen Genet.* 1996;253:217–24.
95. Maguin E, Duwat P, Hege T, Ehrlich D, Gruss A. New thermosensitive plasmid for gram-positive bacteria. *J Bacteriol.* 1992;174:5633–8.
96. Glaser P, Frangeul L, Buchrieser C, Rusniok C, Amend A, Baquero F, et al. Comparative genomics of *Listeria* species. *Science.* 2001;294:849–52.
97. Robinson JT, Thorvaldsdóttir H, Winckler W, Guttman M, Lander ES, Getz G, et al. Integrative Genomics Viewer. *Nat Biotechnol.* 2011;29:24–6.

Supplementary Material

Additional File 1: Supplementary Figure S1. PCA plot for RNA-seq count data. Figure shows the PCA plot for RNA-seq count data for a) strain RO15 all samples, b) strain ScottA all samples, c) RO15 200 MPa samples, d) RO15 400 MPa samples, e) ScottA 200 MPa samples, f) ScottA 200 MPa samples. For both strains we can see a clear separation between treatment and control samples. Each circle represents one sample. Colour representations are given on the right side of the figure.

Additional File 2: Supplementary Figure S2. Number of significantly differentially expressed genes. Figure shows number of differentially expressed genes after pressure treatment for each time point for (a) strain RO15 and (b) strain ScottA. Red bar represents the number of upregulated genes, and the blue bar represents the number of downregulated genes.

Additional File 3: Supplementary Figure S3. The log₂ fold change heatmap of propanediol utilization and cobalamin biosynthesis genes. A) log₂ fold change values for 200 MPa treatment, b) log₂ fold change values for 400 MPa treatment. The gene name and locus tag of genes for R015 and ScottA were given at the end of the row. The log₂ fold change scale is shown at the right corner. In addition, gene homology of cobalamin biosynthesis is shown on the second page.

Additional File 4: Supplementary Figure S4. The log₂ fold change heatmap of transcription factor genes. a) R015 genes, b) ScottA genes, c) ortholog genes for 200 MPa treatment, d) ortholog genes for 400 MPa treatment. The gene name and locus tag of genes for R015 and ScottA are given at the end of the row. The log₂ fold change scale is shown at the right corner.

Additional File 5: Supplementary Figure S5. The log₂ fold change heatmap of transcription machinery genes. a) R015 genes, b) ScottA genes, c) ortholog genes for 200 MPa treatment, d) ortholog genes for 400 MPa treatment. The gene name and locus tag of genes for R015 and ScottA are given at the end of the row. The log₂ fold change scale is shown at the right corner.

Additional File 6: Supplementary Figure S6. The log₂ fold change heatmap of genes of R015 that is not found in ScottA. Locus tag of genes are given at the end of the row. Phage genes were indicated with “phage” text. The log₂ fold change scale is shown at the right corner.

Additional File 7: Supplementary Figure S7. The log₂ fold change heatmap of genes of ScottA that is not found in R015. Locus tag of genes were given at the end of the row. Phage genes were indicated with “phage” text. The log₂ fold change scale is shown at the right corner.

Additional File 8: Supplementary Figure S8. The log₂ fold change heatmap of ncRNA genes. a) log₂ fold change values for 200 MPa treatment, b) log₂ fold change values for 400 MPa treatment. The gene name and locus tag of genes for R015 and ScottA were given at the end of the row. The log₂ fold change scale is shown at the right corner.

Additional File 9: Supplementary Figure S9. ddPCR / RNA-seq correlation for log₂ fold change. The figure shows log₂ fold-changes observed by ddPCR plotted against RNA-seq data for samples of ScottA obtained 10 min after treatment with 400 MPa. Transcripts levels of individual genes obtained by ddPCR were normalized to *recG* levels. Blue circles represent genes that were significantly differentially expressed in both ddPCR and RNA-seq results. White circles represent genes that were not significantly differentially expressed in both ddPCR and RNA-seq. The orange and blue gene names indicate significant up- and down regulation, respectively. The Pearson correlation coefficient between ddPCR and RNA-seq log₂ fold change results was 0.97 (r=0.97).

Additional File 10: Supplementary Figure S10. ddPCR / RNA-seq correlation for log₂ fold change. The figure shows log₂ fold-changes observed by ddPCR plotted against RNA-seq data for samples of ScottA obtained 24 h after treatment with 400 MPa. Transcript levels of individual genes obtained by ddPCR were normalized to *recG* levels. Blue circles represent genes that were significantly differentially expressed in both ddPCR and RNA-seq results. White circles represent genes that were not significantly differentially expressed in both ddPCR and RNA-seq. The orange and blue gene names indicate significant up- and down regulation, respectively. The Pearson correlation coefficient between ddPCR and RNA-seq log₂ fold change results was 0.97 (r=0.97).

Additional File 11: Supplemental Figure S11. Visualization of DNA sequencing reads for strain EGDe, ΔImo1013, and ΔImo2229. a) focused the region includes the gene *lmo1013*, b) focused the region includes the gene *lmo2229*.

Additional File 12: Supplementary Figure S12. Visualization of the experimental design.

Additional File 13: Supplementary Table S1. List of up- and downregulated genes after 200 MPa treatment in R015.

Additional File 14: Supplementary Table S2. List of up- and downregulated genes after 400 MPa treatment in R015.

Additional File 15: Supplementary Table S3. List of up- and downregulated genes after 200 MPa treatment in ScottA.

Additional File 16: Supplementary Table S4. List of up- and downregulated genes after 400 MPa treatment in ScottA.

Additional File 17: Supplementary Table S5. List of enriched GO terms for both up- and downregulated genes after 200 MPa and 400 MPa HPP.

Additional File 18: Supplementary Table S6. 200 MPa and 400 MPa specific upregulated genes in R015. The table is divided into five main columns. First column shows genes upregulated both at 200 MPa and 400 MPa. Second column shows genes upregulated at 200 MPa but not at 400 MPa. Third column shows genes upregulated at 400 MPa but not at 200 MPa. Fourth column shows GO terms enriched for second column genes. Fifth column shows GO terms enriched for third column genes. Time points were divided with sheets.

Additional File 19: Supplementary Table S7. 200 MPa and 400 MPa specific upregulated genes in ScottA. The table is divided into five main columns. First column shows genes upregulated both at 200 MPa and 400 MPa. Second column shows genes upregulated at 200 MPa but not at 400 MPa. Third column shows genes upregulated at 400 MPa but not at 200 MPa. Fourth column shows GO terms enriched for second column genes. Fifth column shows GO terms enriched for third column genes. Time points were divided with sheets.

Additional File 20: Supplementary Table S8. Annotation of ncRNA genes in R015 and RNA-seq read counts for them in R015

Additional File 21: Supplementary Table S9. Annotation of ncRNA genes in R015 and RNA-seq read counts for them in ScottA

Additional File 22: Supplementary Table S10. Table shows gene network link and score of the aggregated network. Undirected links between genes were shown in this table, the third column represents the score of the aggregated network calculated using Seidr. Sheet 1: R015, Sheet 2: ScottA

Additional File 23: Supplementary Table S11. List of clustered genes and cluster links in R015.

Additional File 24: Supplementary Table S12. List of clustered genes and cluster links in ScottA.

Additional File 25: Supplementary Table S13. Significant de novo predicted binding motif from upstream regions of clustered genes in R015. Predicted motifs and upstream region sites were listed. If a database match was seen for the predicted motif, tomtom database results were also listed after the motifs.

Additional File 26: Supplementary Table S14. Significant de novo predicted binding motif from upstream regions of clustered genes in ScottA. Predicted motifs and upstream region sites were listed. If a database match was seen for the predicted motif, tomtom database results were also listed after the motifs.

Additional File 27: Supplementary Table S15. Primers used in ddPCR experiments.

Additional File 28: Supplementary Table S16. Sample IDs used for RNA-seq. Table shows sample IDs and related experimental conditions for both RO15 and ScottA.

Additional File 29: Supplementary Table S17. Raw CDS counts. Table shows raw RNA-seq read counts in CDS in both RO15 and ScottA.

Figures

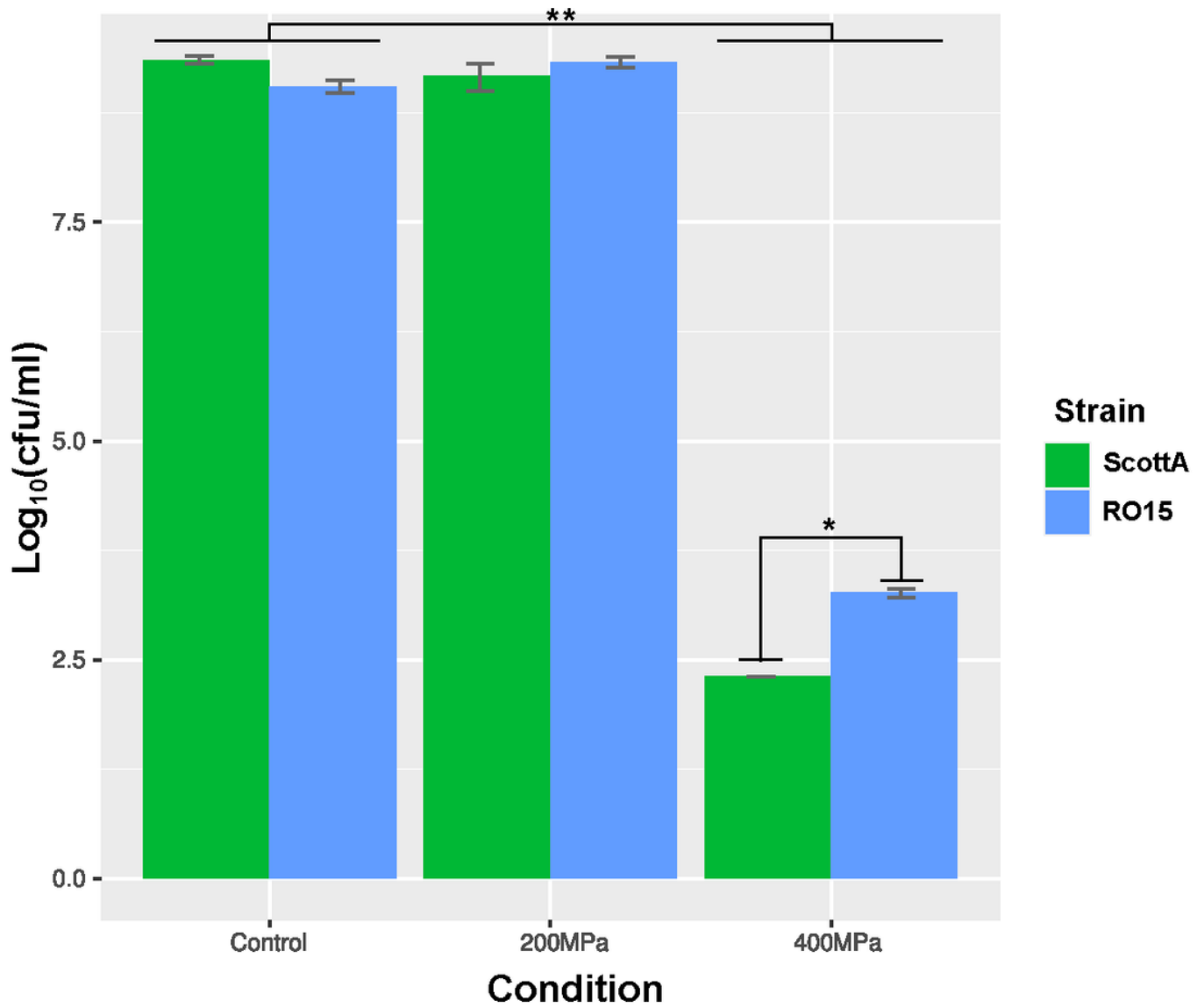


Figure 1

Viable cell count in $\log_{10}(\text{cfu/ml})$ of strain ScottA (green bars) and RO15 (blue bars) after 200 and 400 MPa for 8 min at 8°C. Samples are triplicate (n=3). *: Student's t-test p-value < 0.05 between ScottA and RO15 log reduction. **: Student's t-test p-value < 0.05 between control and 400 MPa $\log(\text{cfu/ml})$ in both strains.

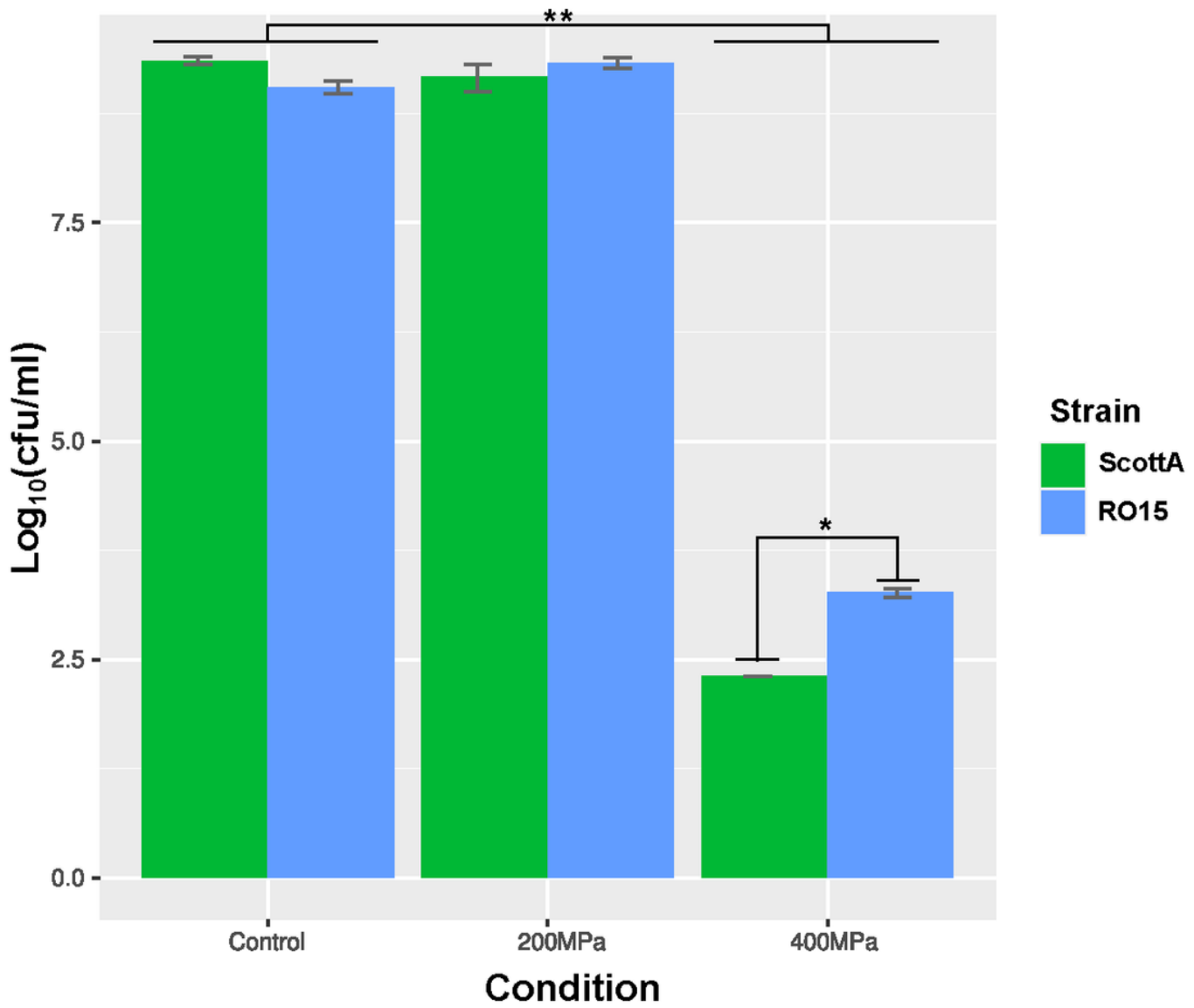


Figure 1

Viable cell count in log₁₀(cfu/ml) of strain ScottA (green bars) and RO15 (blue bars) after 200 and 400 MPa for 8 min at 8°C. Samples are triplicate (n=3). *: Student's t-test p-value < 0.05 between ScottA and RO15 log reduction. **: Student's t-test p-value < 0.05 between control and 400 MPa log(cfu/ml) in both strains.

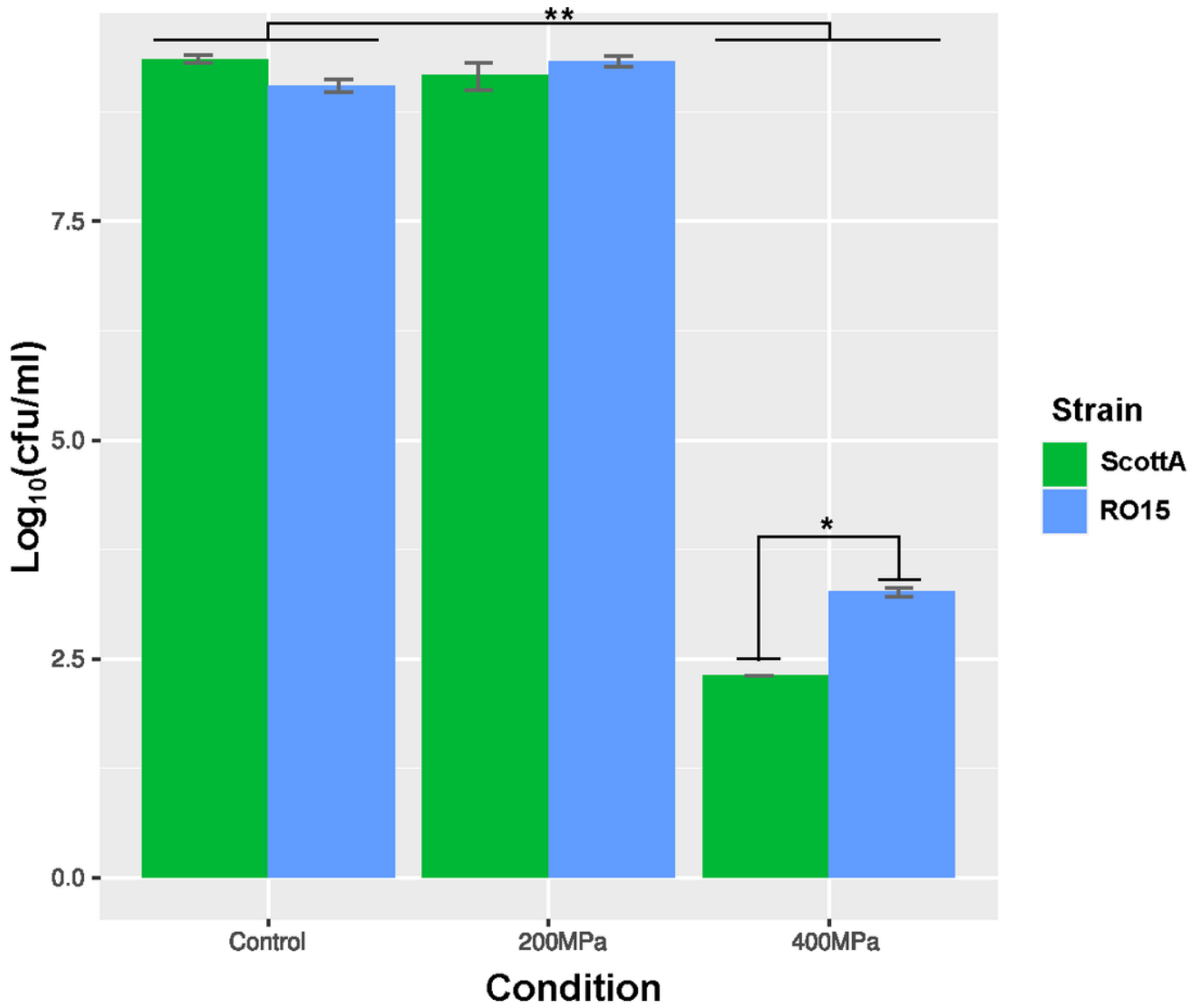
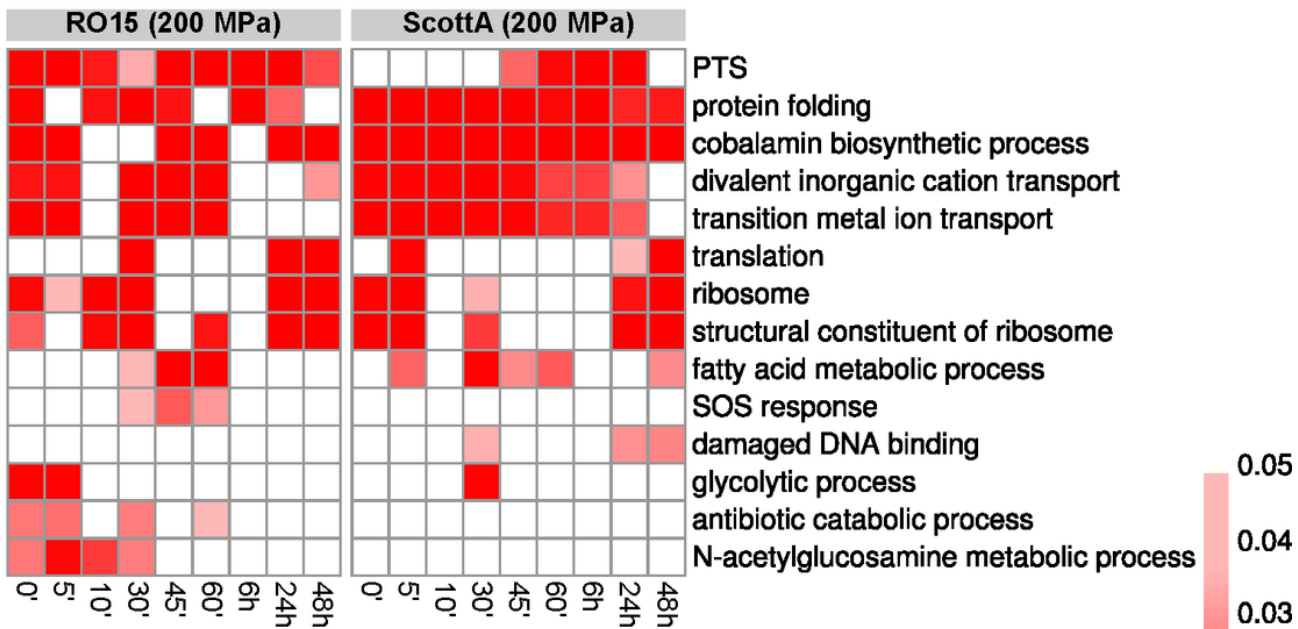


Figure 1

Viable cell count in log₁₀(cfu/ml) of strain ScottA (green bars) and RO15 (blue bars) after 200 and 400 MPa for 8 min at 8°C. Samples are triplicate (n=3). *: Student's t-test p-value < 0.05 between ScottA and RO15 log reduction. **: Student's t-test p-value < 0.05 between control and 400 MPa log(cfu/ml) in both strains.

a) GO enrichment of upregulated genes at 200 MPa



b) GO enrichment of upregulated genes at 400 MPa

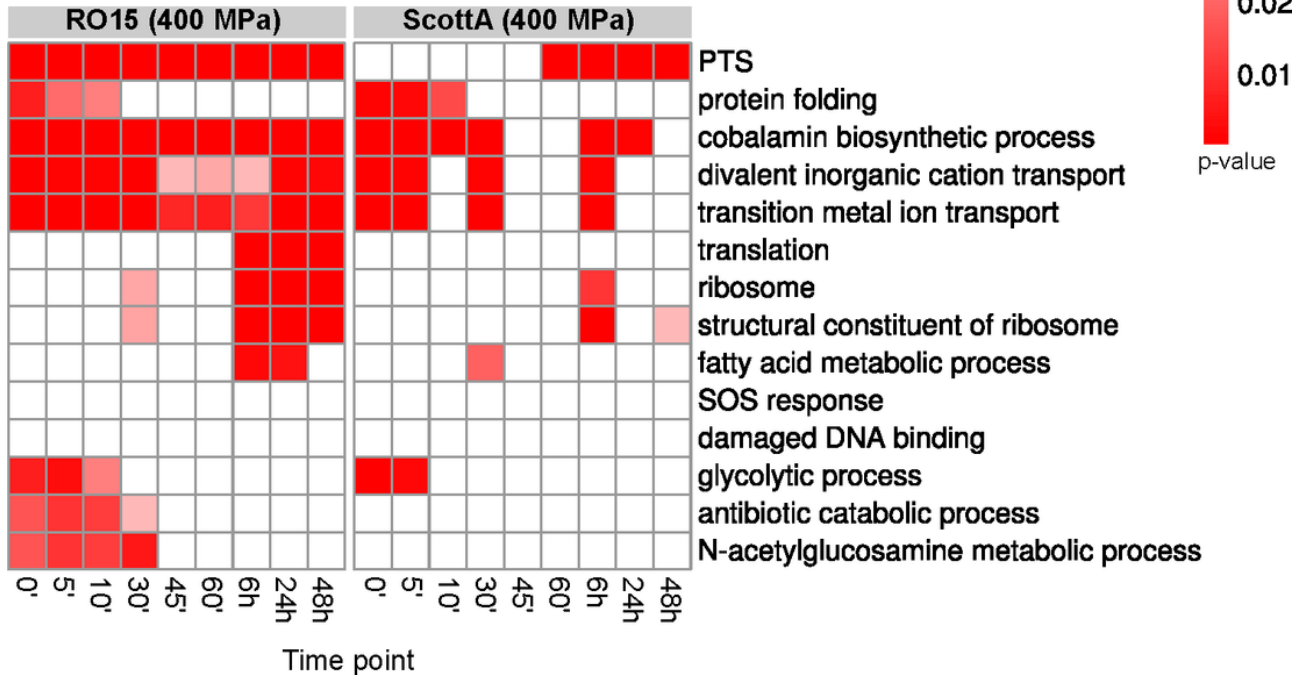
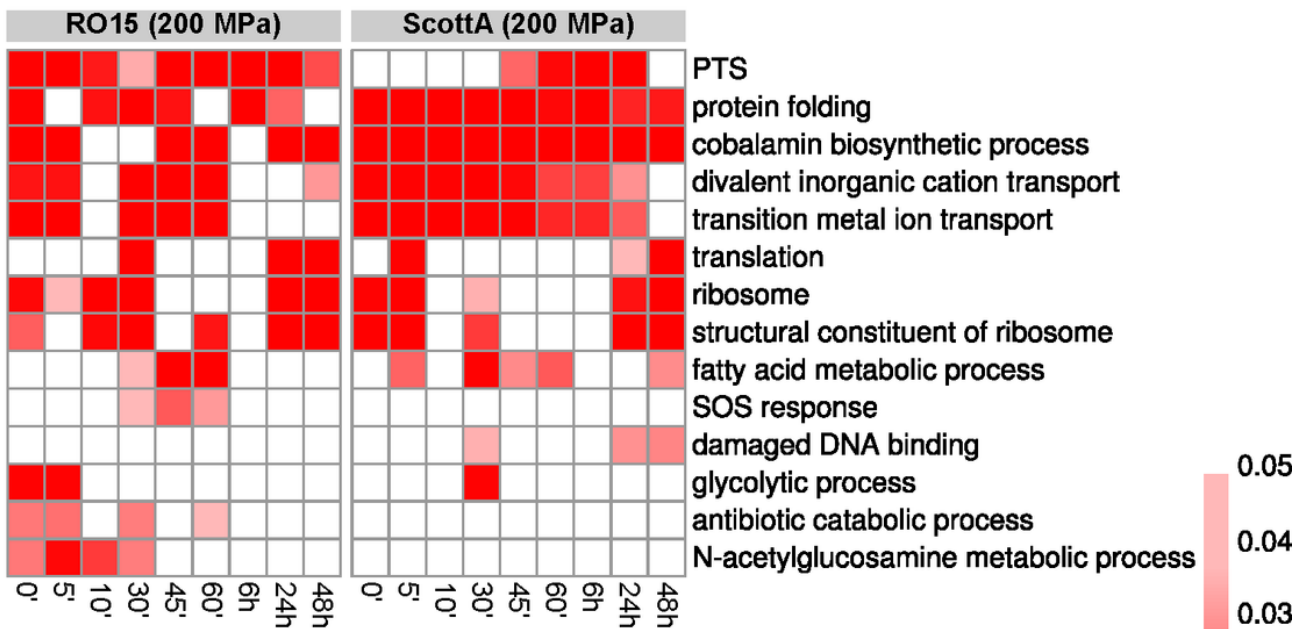


Figure 2

Heat maps of gene ontology (GO) terms enriched in upregulated genes at different timepoints after HPP treatment at a) 200 MPa and b) 400 MPa of *L. monocytogenes* ScottA or RO15. Statistical significance of the GO enrichment (p-values ≤ 0.05) are indicated by a colour gradient (increasing red colour intensity) indicated at the right side of the heat maps). White colour indicates that the GO term was not significantly enriched (p-values > 0.05). For the sake of simplicity, the figure does not include all enriched GO terms, all enriched terms are provided in Table S5.

a) GO enrichment of upregulated genes at 200 MPa



b) GO enrichment of upregulated genes at 400 MPa

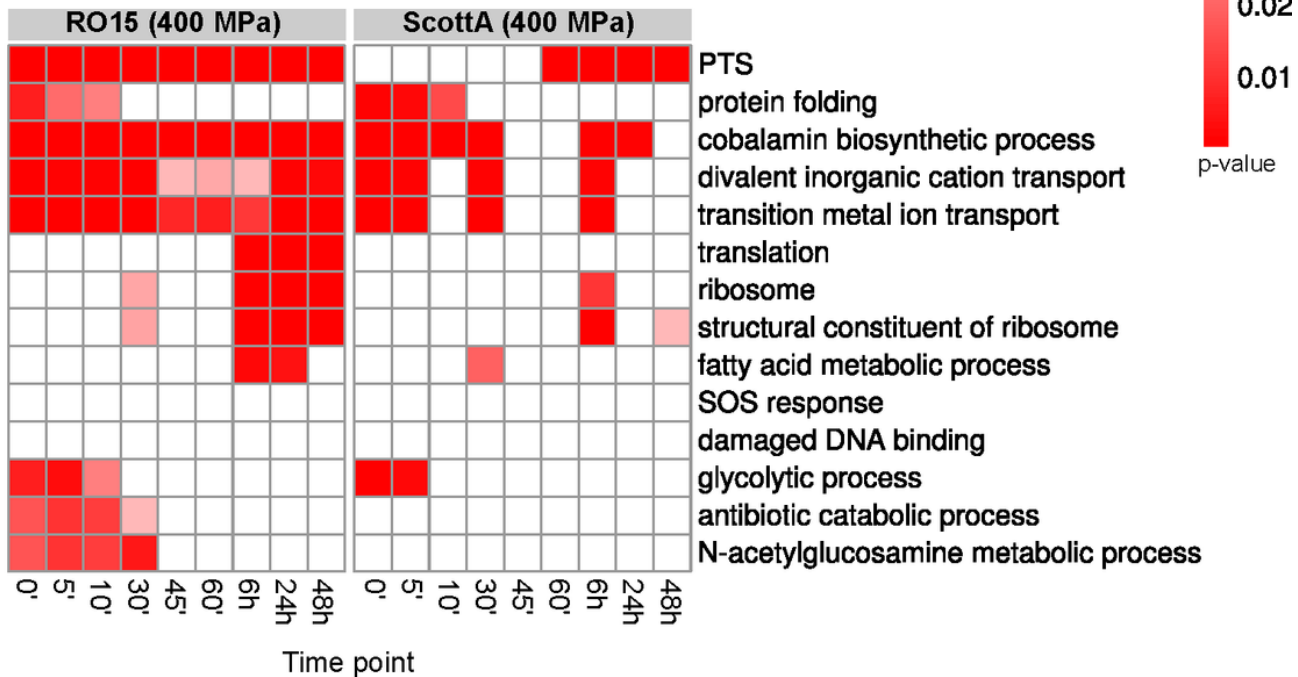
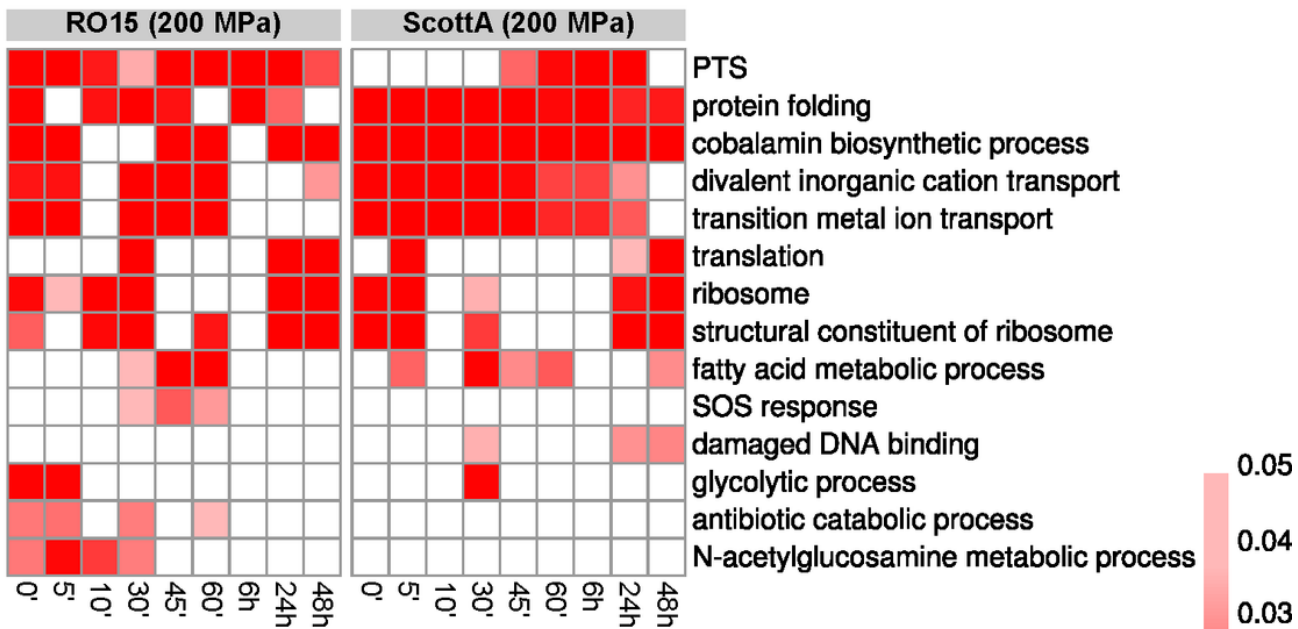


Figure 2

Heat maps of gene ontology (GO) terms enriched in upregulated genes at different timepoints after HPP treatment at a) 200 MPa and b) 400 MPa of *L. monocytogenes* ScottA or RO15. Statistical significance of the GO enrichment (p-values ≤ 0.05) are indicated by a colour gradient (increasing red colour intensity) indicated at the right side of the heat maps). White colour indicates that the GO term was not significantly enriched (p-values > 0.05). For the sake of simplicity, the figure does not include all enriched GO terms, all enriched terms are provided in Table S5.

a) GO enrichment of upregulated genes at 200 MPa



b) GO enrichment of upregulated genes at 400 MPa

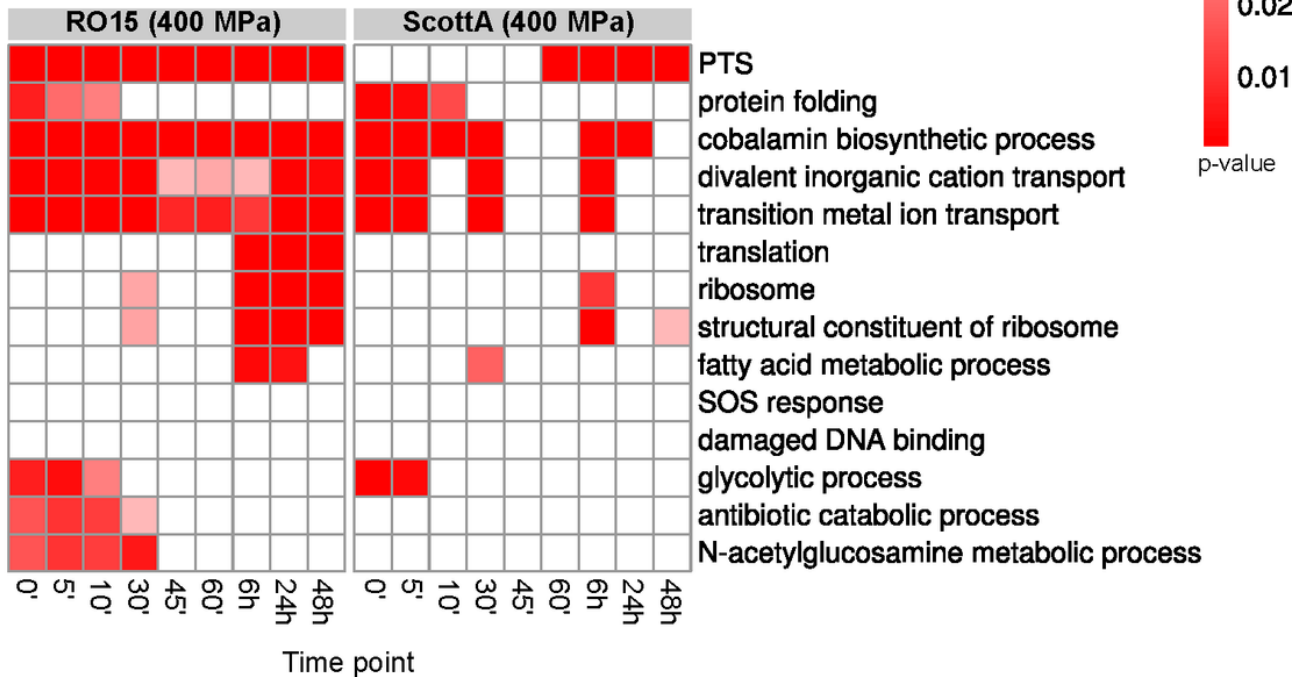


Figure 2

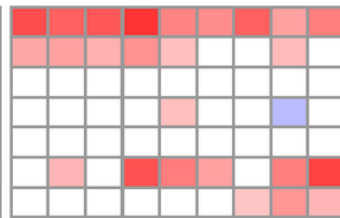
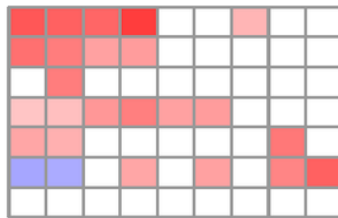
Heat maps of gene ontology (GO) terms enriched in upregulated genes at different timepoints after HPP treatment at a) 200 MPa and b) 400 MPa of *L. monocytogenes* ScottA or RO15. Statistical significance of the GO enrichment (p-values ≤ 0.05) are indicated by a colour gradient (increasing red colour intensity) indicated at the right side of the heat maps). White colour indicates that the GO term was not significantly enriched (p-values > 0.05). For the sake of simplicity, the figure does not include all enriched GO terms, all enriched terms are provided in Table S5.

200MPa

RO15

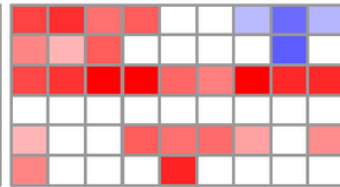
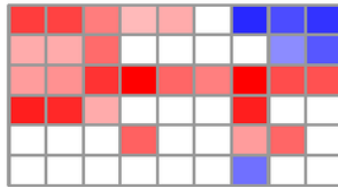
ScottA

a) Peptidoglycan biosynthesis and degradation



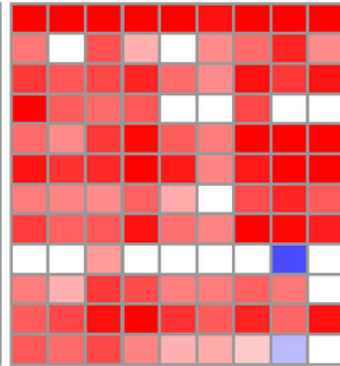
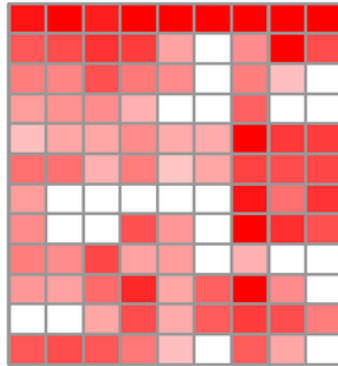
OCPFDLNE_01016 LMOSA_18460 nagA
OCPFDLNE_01017 LMOSA_18470 nagB
OCPFDLNE_02263 LMOSA_960 nagA
OCPFDLNE_02454 LMOSA_3160 nagB
OCPFDLNE_02112 LMOSA_230 murG
OCPFDLNE_02389 LMOSA_2530 pbp2A
OCPFDLNE_01652 LMOSA_25260 murC

b) Transcription factors



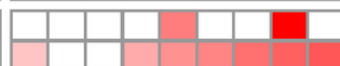
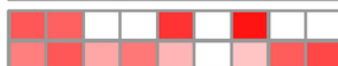
OCPFDLNE_02570 LMOSA_4260 cggR
OCPFDLNE_00204 LMOSA_10930 prfA
OCPFDLNE_01523 LMOSA_23970 hrcA
OCPFDLNE_00442 LMOSA_13240 manR
OCPFDLNE_00248 LMOSA_11270 ctsR
OCPFDLNE_00970 LMOSA_18010 ytrA

c) Chaperones, folding catalysts, peptidases and inhibitors



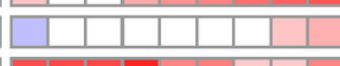
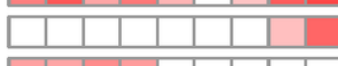
OCPFDLNE_01058 LMOSA_18880 clpE
OCPFDLNE_02312 LMOSA_1410 trxA
OCPFDLNE_02145 LMOSA_550 groEL
OCPFDLNE_02146 LMOSA_560 groES
OCPFDLNE_01521 LMOSA_23950 dnaK
OCPFDLNE_02366 LMOSA_1950 clpB
OCPFDLNE_01520 LMOSA_23940 dnaJ
OCPFDLNE_01522 LMOSA_23960 grpE
OCPFDLNE_02144 LMOSA_540 cbh
OCPFDLNE_01182 LMOSA_20060 clpP
OCPFDLNE_02642 LMOSA_4340 clpP
OCPFDLNE_00287 LMOSA_11680 dapE

d) Antimicrobial resistance



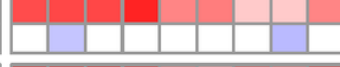
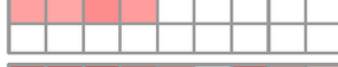
OCPFDLNE_03068 LMOSA_7850 norB
OCPFDLNE_00980 LMOSA_18110 abc-f

e) Cell envelope biosynthesis



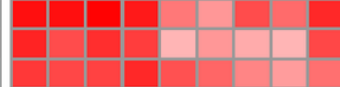
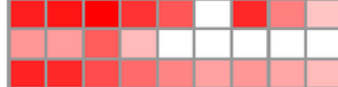
OCPFDLNE_01031 LMOSA_18610 dltD

f) Transcription machinery



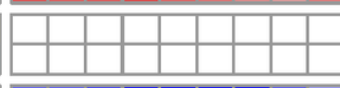
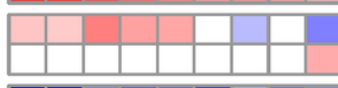
OCPFDLNE_01502 LMOSA_23750 rpoD
OCPFDLNE_00950 LMOSA_17850 sigB

g) Universal stress proteins



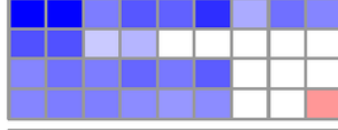
OCPFDLNE_00514 LMOSA_14200 uspA
OCPFDLNE_01628 LMOSA_25020 uspA
OCPFDLNE_02928 LMOSA_6400 uspA

h) Mechanosensitive channels



OCPFDLNE_02141 LMOSA_510 mscL
OCPFDLNE_01076 LMOSA_19040 ykuT

i) Cell division



OCPFDLNE_00221 LMOSA_11100 divIC
OCPFDLNE_02096 LMOSA_29350 divIVA
OCPFDLNE_02681 LMOSA_4730ftsE
OCPFDLNE_02680 LMOSA_4720ftsX

j) Ribosome hibernation



OCPFDLNE_02685 LMOSA_4770 hpf

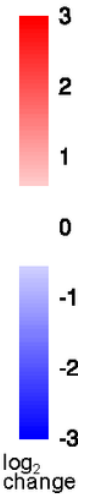


Figure 3

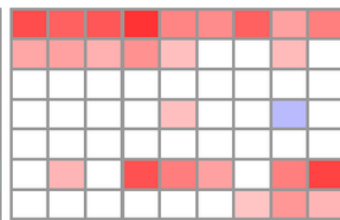
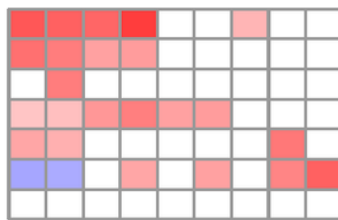
Heat maps with log₂ fold-change of selected genes in selected gene families in *L. monocytogenes* RO15 or ScottA after 200 MPa pressure treatment. Gene names and locus tags for RO15 and ScottA are indicated at the end of each row. Log₂ fold-change scale is shown in the right corner.

200MPa

RO15

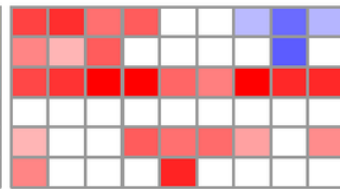
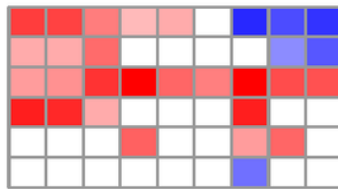
ScottA

a) Peptidoglycan biosynthesis and degradation



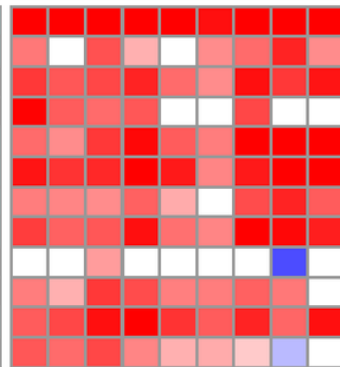
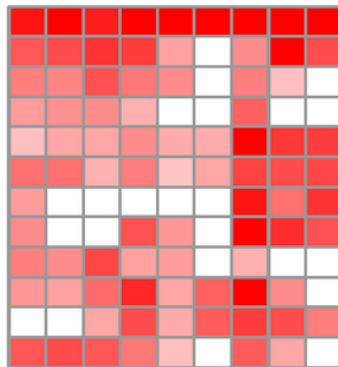
OCPFDLNE_01016 LMOSA_18460 nagA
 OCPFDLNE_01017 LMOSA_18470 nagB
 OCPFDLNE_02263 LMOSA_960 nagA
 OCPFDLNE_02454 LMOSA_3160 nagB
 OCPFDLNE_02112 LMOSA_230 murG
 OCPFDLNE_02389 LMOSA_2530 pbp2A
 OCPFDLNE_01652 LMOSA_25260 murC

b) Transcription factors



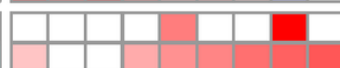
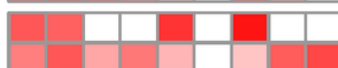
OCPFDLNE_02570 LMOSA_4260 cggR
 OCPFDLNE_00204 LMOSA_10930 prfA
 OCPFDLNE_01523 LMOSA_23970 hrcA
 OCPFDLNE_00442 LMOSA_13240 manR
 OCPFDLNE_00248 LMOSA_11270 ctsR
 OCPFDLNE_00970 LMOSA_18010 ytrA

c) Chaperones, folding catalysts, peptidases and inhibitors



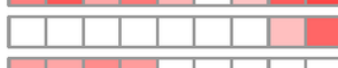
OCPFDLNE_01058 LMOSA_18880 clpE
 OCPFDLNE_02312 LMOSA_1410 trxA
 OCPFDLNE_02145 LMOSA_550 groEL
 OCPFDLNE_02146 LMOSA_560 groES
 OCPFDLNE_01521 LMOSA_23950 dnaK
 OCPFDLNE_02366 LMOSA_1950 clpB
 OCPFDLNE_01520 LMOSA_23940 dnaJ
 OCPFDLNE_01522 LMOSA_23960 grpE
 OCPFDLNE_02144 LMOSA_540 cbh
 OCPFDLNE_01182 LMOSA_20060 clpP
 OCPFDLNE_02642 LMOSA_4340 clpP
 OCPFDLNE_00287 LMOSA_11680 dapE

d) Antimicrobial resistance



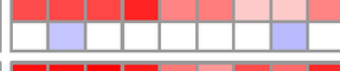
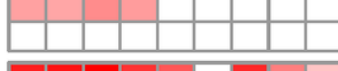
OCPFDLNE_03068 LMOSA_7850 norB
 OCPFDLNE_00980 LMOSA_18110 abc-f

e) Cell envelope biosynthesis



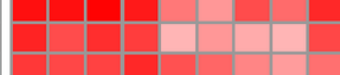
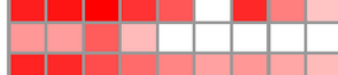
OCPFDLNE_01031 LMOSA_18610 dltD

f) Transcription machinery



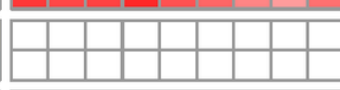
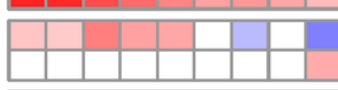
OCPFDLNE_01502 LMOSA_23750 rpoD
 OCPFDLNE_00950 LMOSA_17850 sigB

g) Universal stress proteins



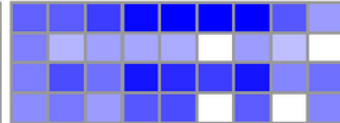
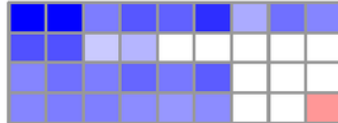
OCPFDLNE_00514 LMOSA_14200 uspA
 OCPFDLNE_01628 LMOSA_25020 uspA
 OCPFDLNE_02928 LMOSA_6400 uspA

h) Mechanosensitive channels



OCPFDLNE_02141 LMOSA_510 mscL
 OCPFDLNE_01076 LMOSA_19040 ykuT

i) Cell division



OCPFDLNE_00221 LMOSA_11100 divIC
 OCPFDLNE_02096 LMOSA_29350 divIVA
 OCPFDLNE_02681 LMOSA_4730ftsE
 OCPFDLNE_02680 LMOSA_4720ftsX

j) Ribosome hibernation



OCPFDLNE_02685 LMOSA_4770 hpf

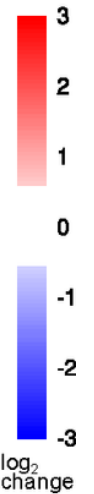


Figure 3

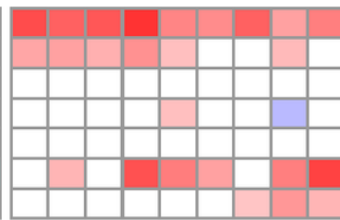
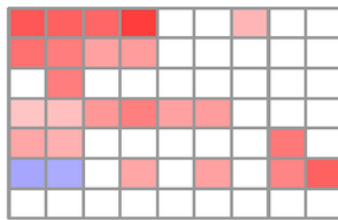
Heat maps with log₂ fold-change of selected genes in selected gene families in *L. monocytogenes* RO15 or ScottA after 200 MPa pressure treatment. Gene names and locus tags for RO15 and ScottA are indicated at the end of each row. Log₂ fold-change scale is shown in the right corner.

200MPa

RO15

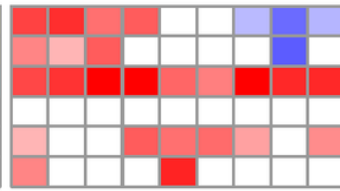
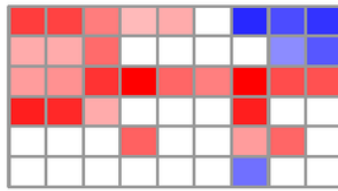
ScottA

a) Peptidoglycan biosynthesis and degradation



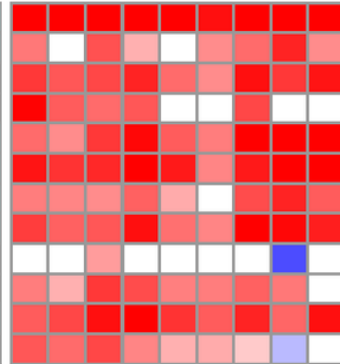
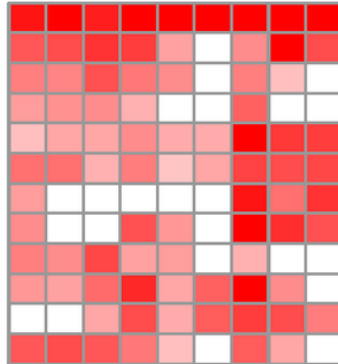
OCPFDLNE_01016 LMOSA_18460 nagA
 OCPFDLNE_01017 LMOSA_18470 nagB
 OCPFDLNE_02263 LMOSA_960 nagA
 OCPFDLNE_02454 LMOSA_3160 nagB
 OCPFDLNE_02112 LMOSA_230 murG
 OCPFDLNE_02389 LMOSA_2530 pbp2A
 OCPFDLNE_01652 LMOSA_25260 murC

b) Transcription factors



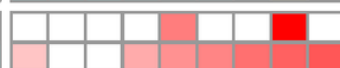
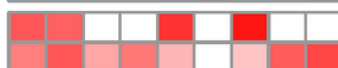
OCPFDLNE_02570 LMOSA_4260 cggR
 OCPFDLNE_00204 LMOSA_10930 prfA
 OCPFDLNE_01523 LMOSA_23970 hrcA
 OCPFDLNE_00442 LMOSA_13240 manR
 OCPFDLNE_00248 LMOSA_11270 ctsR
 OCPFDLNE_00970 LMOSA_18010 ytrA

c) Chaperones, folding catalysts, peptidases and inhibitors



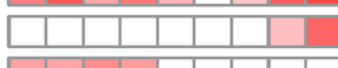
OCPFDLNE_01058 LMOSA_18880 clpE
 OCPFDLNE_02312 LMOSA_1410 trxA
 OCPFDLNE_02145 LMOSA_550 groEL
 OCPFDLNE_02146 LMOSA_560 groES
 OCPFDLNE_01521 LMOSA_23950 dnaK
 OCPFDLNE_02366 LMOSA_1950 clpB
 OCPFDLNE_01520 LMOSA_23940 dnaJ
 OCPFDLNE_01522 LMOSA_23960 grpE
 OCPFDLNE_02144 LMOSA_540 cbh
 OCPFDLNE_01182 LMOSA_20060 clpP
 OCPFDLNE_02642 LMOSA_4340 clpP
 OCPFDLNE_00287 LMOSA_11680 dapE

d) Antimicrobial resistance



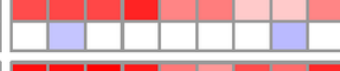
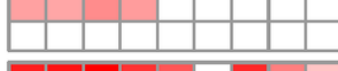
OCPFDLNE_03068 LMOSA_7850 norB
 OCPFDLNE_00980 LMOSA_18110 abc-f

e) Cell envelope biosynthesis



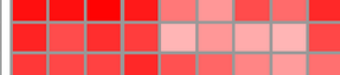
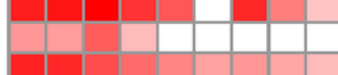
OCPFDLNE_01031 LMOSA_18610 dltD

f) Transcription machinery



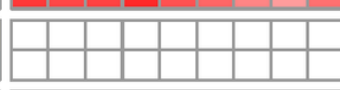
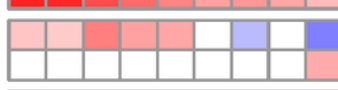
OCPFDLNE_01502 LMOSA_23750 rpoD
 OCPFDLNE_00950 LMOSA_17850 sigB

g) Universal stress proteins



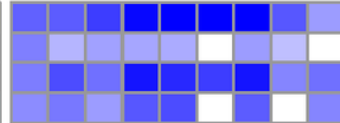
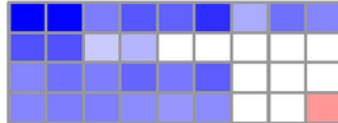
OCPFDLNE_00514 LMOSA_14200 uspA
 OCPFDLNE_01628 LMOSA_25020 uspA
 OCPFDLNE_02928 LMOSA_6400 uspA

h) Mechanosensitive channels



OCPFDLNE_02141 LMOSA_510 mscL
 OCPFDLNE_01076 LMOSA_19040 ykuT

i) Cell division



OCPFDLNE_00221 LMOSA_11100 divIC
 OCPFDLNE_02096 LMOSA_29350 divIVA
 OCPFDLNE_02681 LMOSA_4730ftsE
 OCPFDLNE_02680 LMOSA_4720ftsX

j) Ribosome hibernation



OCPFDLNE_02685 LMOSA_4770 hpf

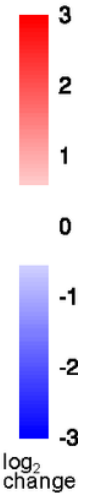


Figure 3

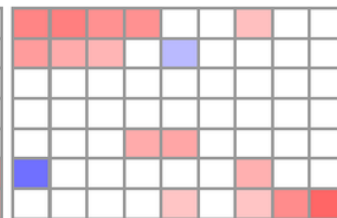
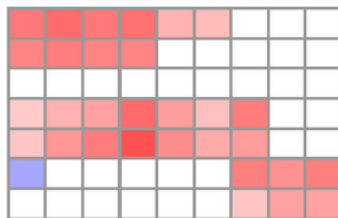
Heat maps with log₂ fold-change of selected genes in selected gene families in *L. monocytogenes* RO15 or ScottA after 200 MPa pressure treatment. Gene names and locus tags for RO15 and ScottA are indicated at the end of each row. Log₂ fold-change scale is shown in the right corner.

400MPa

RO15

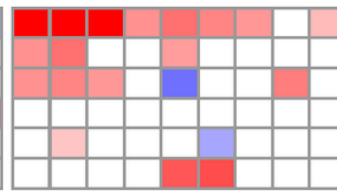
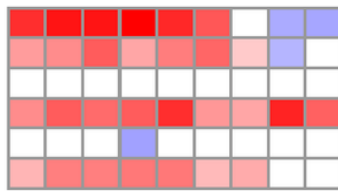
ScottA

a) Peptidoglycan biosynthesis and degradation



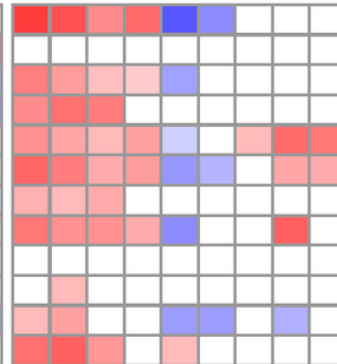
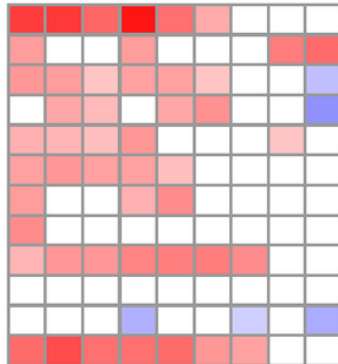
OCPFDLNE_01016 LMOSA_18460 nagA
OCPFDLNE_01017 LMOSA_18470 nagB
OCPFDLNE_02263 LMOSA_960 nagA
OCPFDLNE_02454 LMOSA_3160 nagB
OCPFDLNE_02112 LMOSA_230 murG
OCPFDLNE_02389 LMOSA_2530 pbp2A
OCPFDLNE_01652 LMOSA_25260 murC

b) Transcription factors



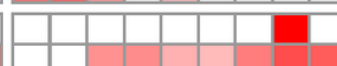
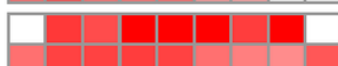
OCPFDLNE_02570 LMOSA_4260 cggR
OCPFDLNE_00204 LMOSA_10930 prfA
OCPFDLNE_01523 LMOSA_23970 hrcA
OCPFDLNE_00442 LMOSA_13240 manR
OCPFDLNE_00248 LMOSA_11270 ctsR
OCPFDLNE_00970 LMOSA_18010 ytrA

c) Chaperones, folding catalysts, peptidases and inhibitors



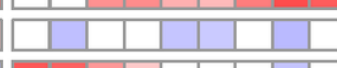
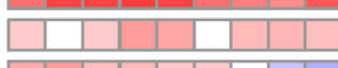
OCPFDLNE_01058 LMOSA_18880 clpE
OCPFDLNE_02312 LMOSA_1410 trxA
OCPFDLNE_02145 LMOSA_550 groEL
OCPFDLNE_02146 LMOSA_560 groES
OCPFDLNE_01521 LMOSA_23950 dnaK
OCPFDLNE_02366 LMOSA_1950 clpB
OCPFDLNE_01520 LMOSA_23940 dnaJ
OCPFDLNE_01522 LMOSA_23960 grpE
OCPFDLNE_02144 LMOSA_540 cbh
OCPFDLNE_01182 LMOSA_20060 clpP
OCPFDLNE_02642 LMOSA_4340 clpP
OCPFDLNE_00287 LMOSA_11680 dapE

d) Antimicrobial resistance



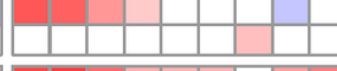
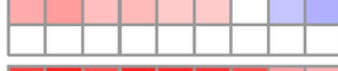
OCPFDLNE_03068 LMOSA_7850 norB
OCPFDLNE_00980 LMOSA_18110 abc-f

e) Cell envelope biosynthesis



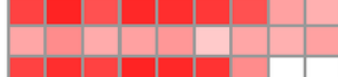
OCPFDLNE_01031 LMOSA_18610 dltD

f) Transcription machinery



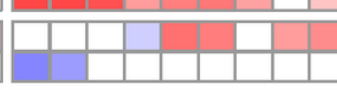
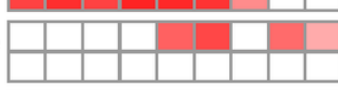
OCPFDLNE_01502 LMOSA_23750 rpoD
OCPFDLNE_00950 LMOSA_17850 sigB

g) Universal stress proteins



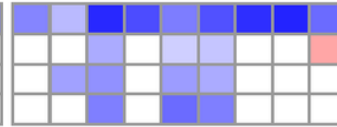
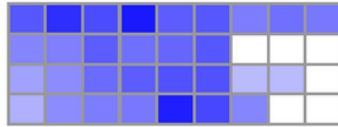
OCPFDLNE_00514 LMOSA_14200 uspA
OCPFDLNE_01628 LMOSA_25020 uspA
OCPFDLNE_02928 LMOSA_6400 uspA

h) Mechanosensitive channels



OCPFDLNE_02141 LMOSA_510 mscL
OCPFDLNE_01076 LMOSA_19040 ykuT

i) Cell division



OCPFDLNE_00221 LMOSA_11100 divIC
OCPFDLNE_02096 LMOSA_29350 divIVA
OCPFDLNE_02681 LMOSA_4730 ftsE
OCPFDLNE_02680 LMOSA_4720 ftsX

j) Ribosome hibernation



OCPFDLNE_02685 LMOSA_4770 hpf

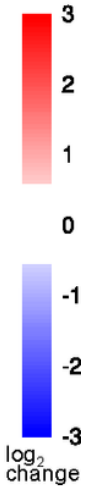


Figure 4

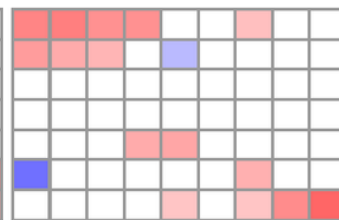
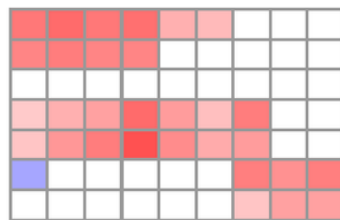
Heat maps with log₂ fold changes of selected genes of selected gene families in *L. monocytogenes* RO15 or ScottA after 400 MPa pressure treatment. The gene name and locus tag of genes for RO15 and ScottA are given at the end of the row. The log₂ fold change scale is shown in the right corner.

400MPa

RO15

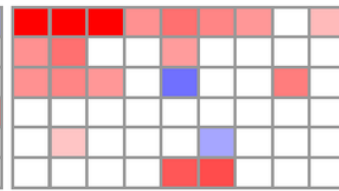
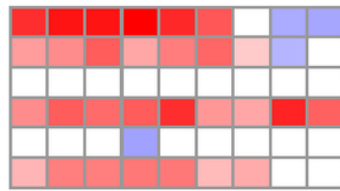
ScottA

a) Peptidoglycan biosynthesis and degradation



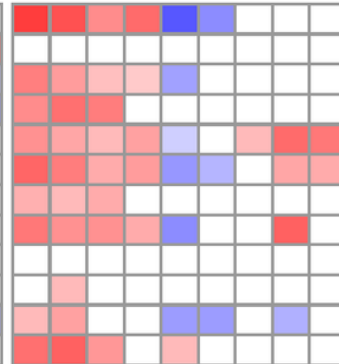
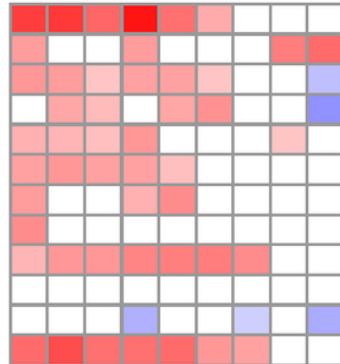
OCPFDLNE_01016 LMOSA_18460 nagA
 OCPFDLNE_01017 LMOSA_18470 nagB
 OCPFDLNE_02263 LMOSA_960 nagA
 OCPFDLNE_02454 LMOSA_3160 nagB
 OCPFDLNE_02112 LMOSA_230 murG
 OCPFDLNE_02389 LMOSA_2530 pbp2A
 OCPFDLNE_01652 LMOSA_25260 murC

b) Transcription factors



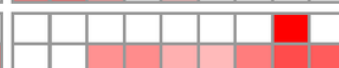
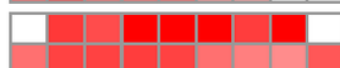
OCPFDLNE_02570 LMOSA_4260 cggR
 OCPFDLNE_00204 LMOSA_10930 prfA
 OCPFDLNE_01523 LMOSA_23970 hrcA
 OCPFDLNE_00442 LMOSA_13240 manR
 OCPFDLNE_00248 LMOSA_11270 ctsR
 OCPFDLNE_00970 LMOSA_18010 ytrA

c) Chaperones, folding catalysts, peptidases and inhibitors



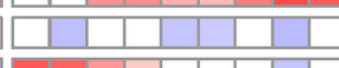
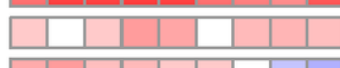
OCPFDLNE_01058 LMOSA_18880 clpE
 OCPFDLNE_02312 LMOSA_1410 trxA
 OCPFDLNE_02145 LMOSA_550 groEL
 OCPFDLNE_02146 LMOSA_560 groES
 OCPFDLNE_01521 LMOSA_23950 dnaK
 OCPFDLNE_02366 LMOSA_1950 clpB
 OCPFDLNE_01520 LMOSA_23940 dnaJ
 OCPFDLNE_01522 LMOSA_23960 grpE
 OCPFDLNE_02144 LMOSA_540 cbh
 OCPFDLNE_01182 LMOSA_20060 clpP
 OCPFDLNE_02642 LMOSA_4340 clpP
 OCPFDLNE_00287 LMOSA_11680 dapE

d) Antimicrobial resistance



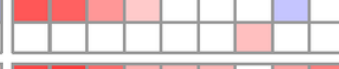
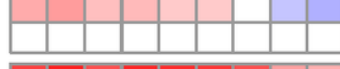
OCPFDLNE_03068 LMOSA_7850 norB
 OCPFDLNE_00980 LMOSA_18110 abc-f

e) Cell envelope biosynthesis



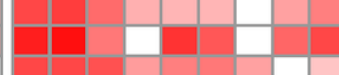
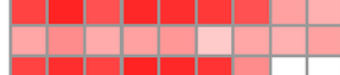
OCPFDLNE_01031 LMOSA_18610 dltD

f) Transcription machinery



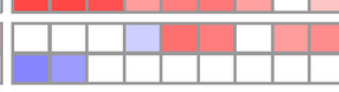
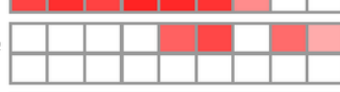
OCPFDLNE_01502 LMOSA_23750 rpoD
 OCPFDLNE_00950 LMOSA_17850 sigB

g) Universal stress proteins



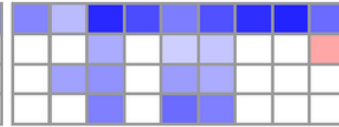
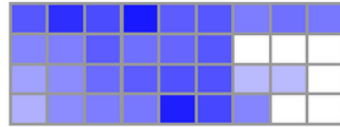
OCPFDLNE_00514 LMOSA_14200 uspA
 OCPFDLNE_01628 LMOSA_25020 uspA
 OCPFDLNE_02928 LMOSA_6400 uspA

h) Mechanosensitive channels



OCPFDLNE_02141 LMOSA_510 mscL
 OCPFDLNE_01076 LMOSA_19040 ykuT

i) Cell division



OCPFDLNE_00221 LMOSA_11100 divIC
 OCPFDLNE_02096 LMOSA_29350 divIVA
 OCPFDLNE_02681 LMOSA_4730 ftsE
 OCPFDLNE_02680 LMOSA_4720 ftsX

j) Ribosome hibernation



OCPFDLNE_02685 LMOSA_4770 hpf

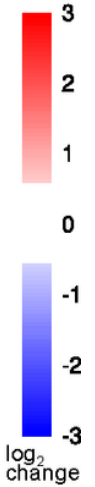


Figure 4

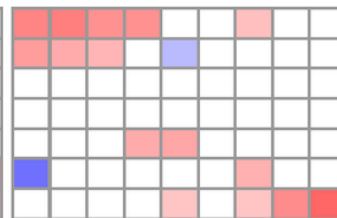
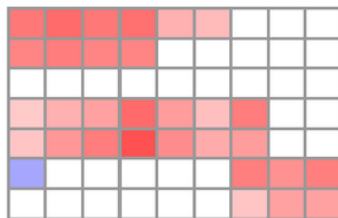
Heat maps with log₂ fold changes of selected genes of selected gene families in *L. monocytogenes* RO15 or ScottA after 400 MPa pressure treatment. The gene name and locus tag of genes for RO15 and ScottA are given at the end of the row. The log₂ fold change scale is shown in the right corner.

400MPa

RO15

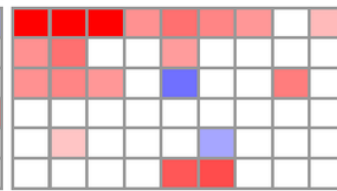
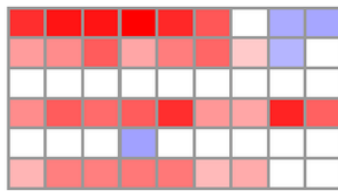
ScottA

a) Peptidoglycan biosynthesis and degradation



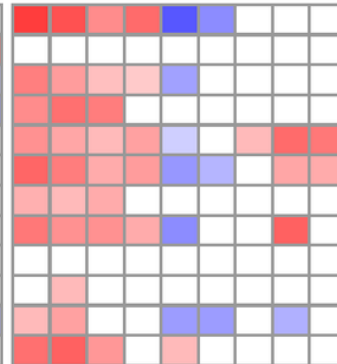
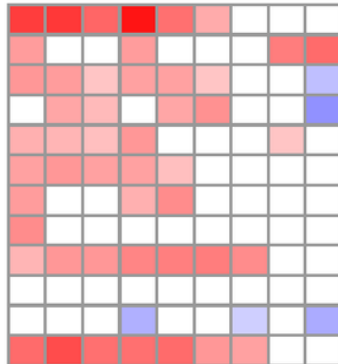
OCPFDLNE_01016 LMOSA_18460 nagA
 OCPFDLNE_01017 LMOSA_18470 nagB
 OCPFDLNE_02263 LMOSA_960 nagA
 OCPFDLNE_02454 LMOSA_3160 nagB
 OCPFDLNE_02112 LMOSA_230 murG
 OCPFDLNE_02389 LMOSA_2530 pbp2A
 OCPFDLNE_01652 LMOSA_25260 murC

b) Transcription factors



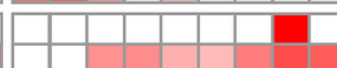
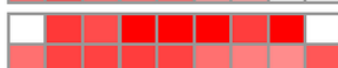
OCPFDLNE_02570 LMOSA_4260 cggR
 OCPFDLNE_00204 LMOSA_10930 prfA
 OCPFDLNE_01523 LMOSA_23970 hrcA
 OCPFDLNE_00442 LMOSA_13240 manR
 OCPFDLNE_00248 LMOSA_11270 ctsR
 OCPFDLNE_00970 LMOSA_18010 ytrA

c) Chaperones, folding catalysts, peptidases and inhibitors



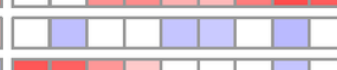
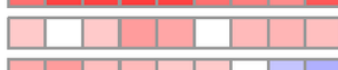
OCPFDLNE_01058 LMOSA_18880 clpE
 OCPFDLNE_02312 LMOSA_1410 trxA
 OCPFDLNE_02145 LMOSA_550 groEL
 OCPFDLNE_02146 LMOSA_560 groES
 OCPFDLNE_01521 LMOSA_23950 dnaK
 OCPFDLNE_02366 LMOSA_1950 clpB
 OCPFDLNE_01520 LMOSA_23940 dnaJ
 OCPFDLNE_01522 LMOSA_23960 grpE
 OCPFDLNE_02144 LMOSA_540 cbh
 OCPFDLNE_01182 LMOSA_20060 clpP
 OCPFDLNE_02642 LMOSA_4340 clpP
 OCPFDLNE_00287 LMOSA_11680 dapE

d) Antimicrobial resistance



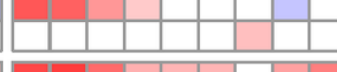
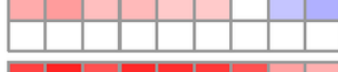
OCPFDLNE_03068 LMOSA_7850 norB
 OCPFDLNE_00980 LMOSA_18110 abc-f

e) Cell envelope biosynthesis



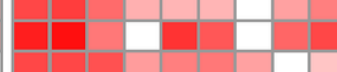
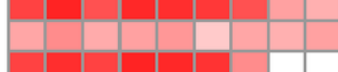
OCPFDLNE_01031 LMOSA_18610 dltD

f) Transcription machinery



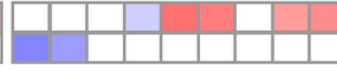
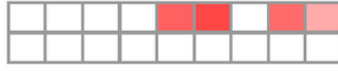
OCPFDLNE_01502 LMOSA_23750 rpoD
 OCPFDLNE_00950 LMOSA_17850 sigB

g) Universal stress proteins



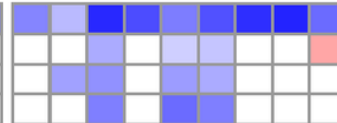
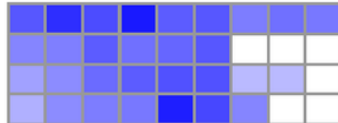
OCPFDLNE_00514 LMOSA_14200 uspA
 OCPFDLNE_01628 LMOSA_25020 uspA
 OCPFDLNE_02928 LMOSA_6400 uspA

h) Mechanosensitive channels



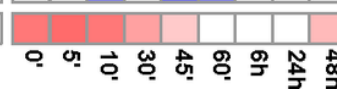
OCPFDLNE_02141 LMOSA_510 mscL
 OCPFDLNE_01076 LMOSA_19040 ykuT

i) Cell division



OCPFDLNE_00221 LMOSA_11100 divIC
 OCPFDLNE_02096 LMOSA_29350 divIVA
 OCPFDLNE_02681 LMOSA_4730 ftsE
 OCPFDLNE_02680 LMOSA_4720 ftsX

j) Ribosome hibernation



OCPFDLNE_02685 LMOSA_4770 hpf

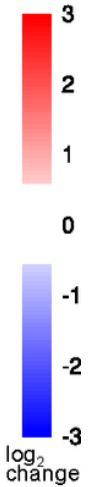


Figure 4

Heat maps with log₂ fold changes of selected genes of selected gene families in *L. monocytogenes* RO15 or ScottA after 400 MPa pressure treatment. The gene name and locus tag of genes for RO15 and ScottA are given at the end of the row. The log₂ fold change scale is shown in the right corner.

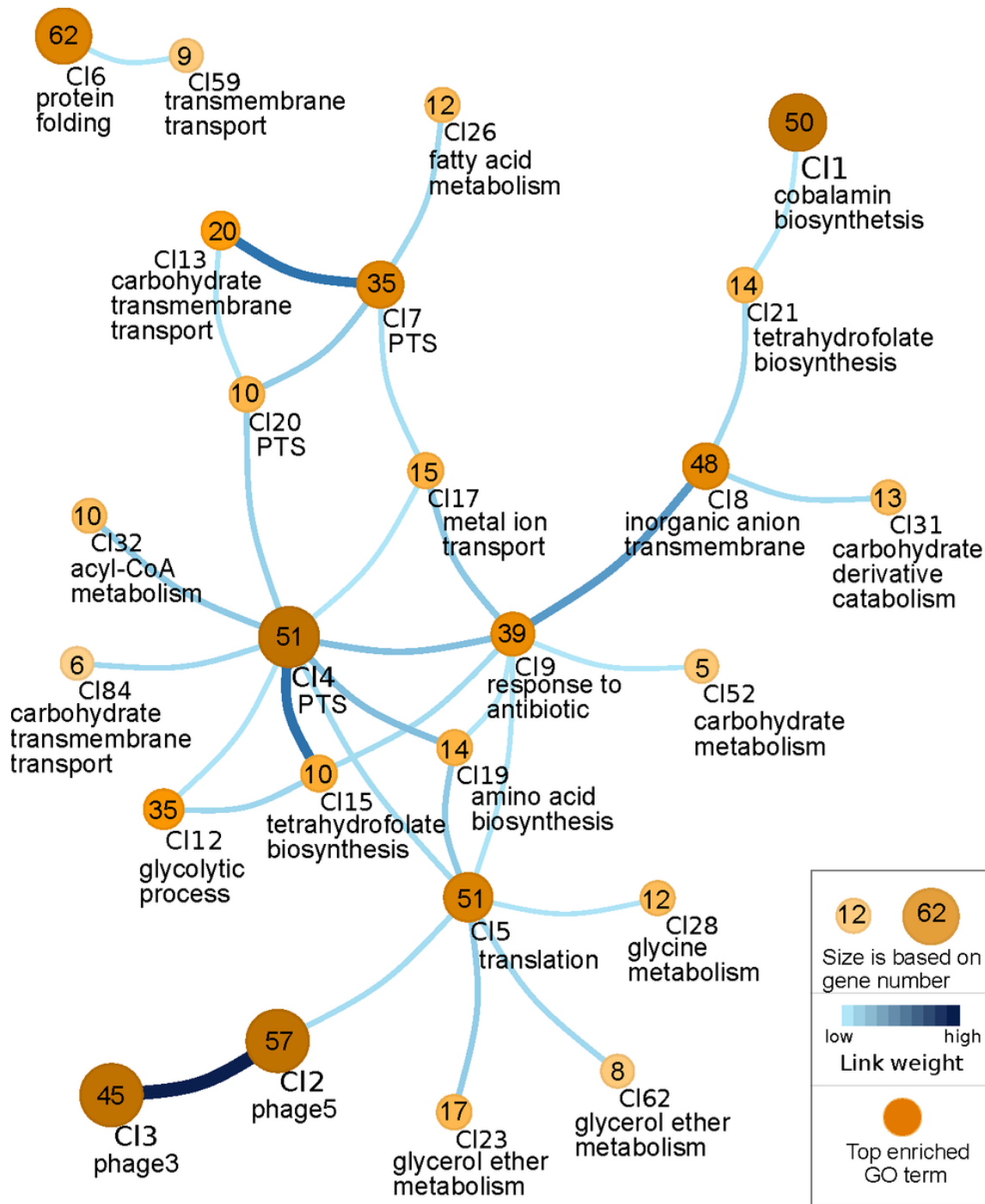


Figure 5

Visualization of clustered genes based on gene network inference in *L. monocytogenes* R015. Each node represents a cluster and edges represent predicted links between clusters. Number of genes within the clusters is shown in the center of the node. Below the cluster, the top-scored enriched GO term is given. The used scales are described in the box. Size and colour are based on gene number. For simplification, the figure shows only the top 30 links with the highest weight, and their connected clusters. Genes within the clusters, and all links between clusters, are listed in Table S11.

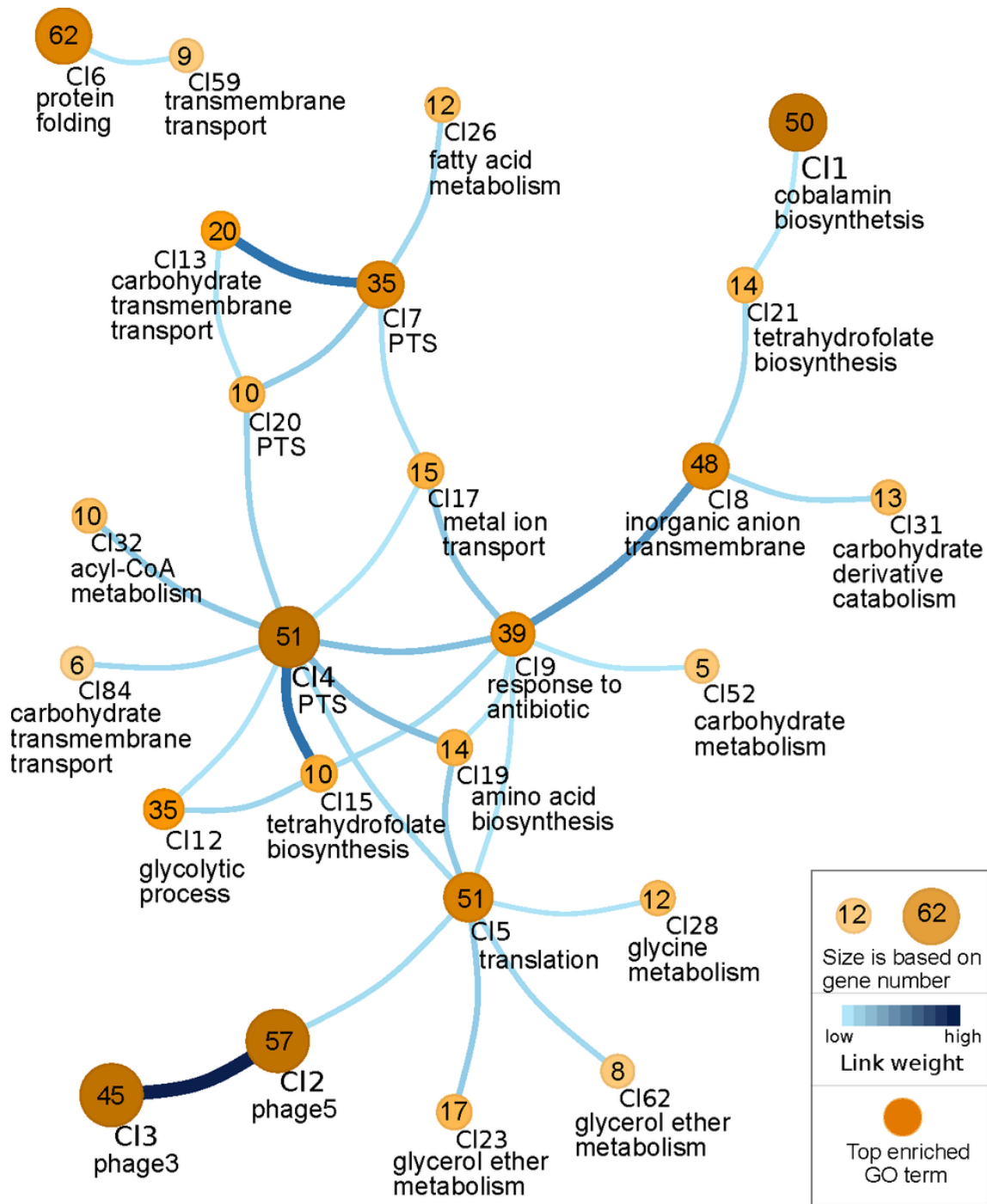


Figure 5

Visualization of clustered genes based on gene network inference in *L. monocytogenes* R015. Each node represents a cluster and edges represent predicted links between clusters. Number of genes within the clusters is shown in the center of the node. Below the cluster, the top-scored enriched GO term is given. The used scales are described in the box. Size and colour are based on gene number. For simplification, the figure shows only the top 30 links with the highest weight, and their connected clusters. Genes within the clusters, and all links between clusters, are listed in Table S11.

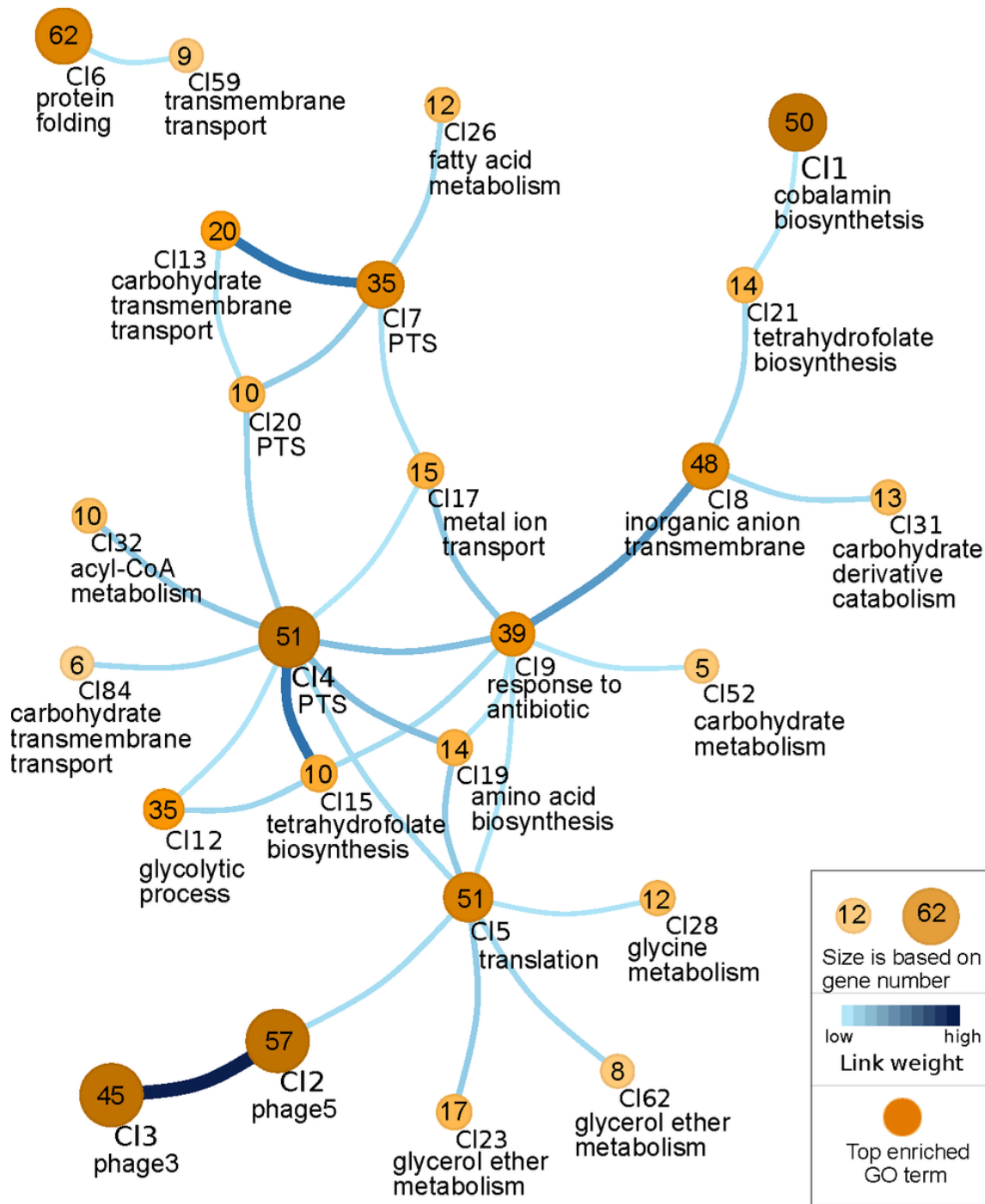


Figure 5

Visualization of clustered genes based on gene network inference in *L. monocytogenes* R015. Each node represents a cluster and edges represent predicted links between clusters. Number of genes within the clusters is shown in the center of the node. Below the cluster, the top-scored enriched GO term is given. The used scales are described in the box. Size and colour are based on gene number. For simplification, the figure shows only the top 30 links with the highest weight, and their connected clusters. Genes within the clusters, and all links between clusters, are listed in Table S11.

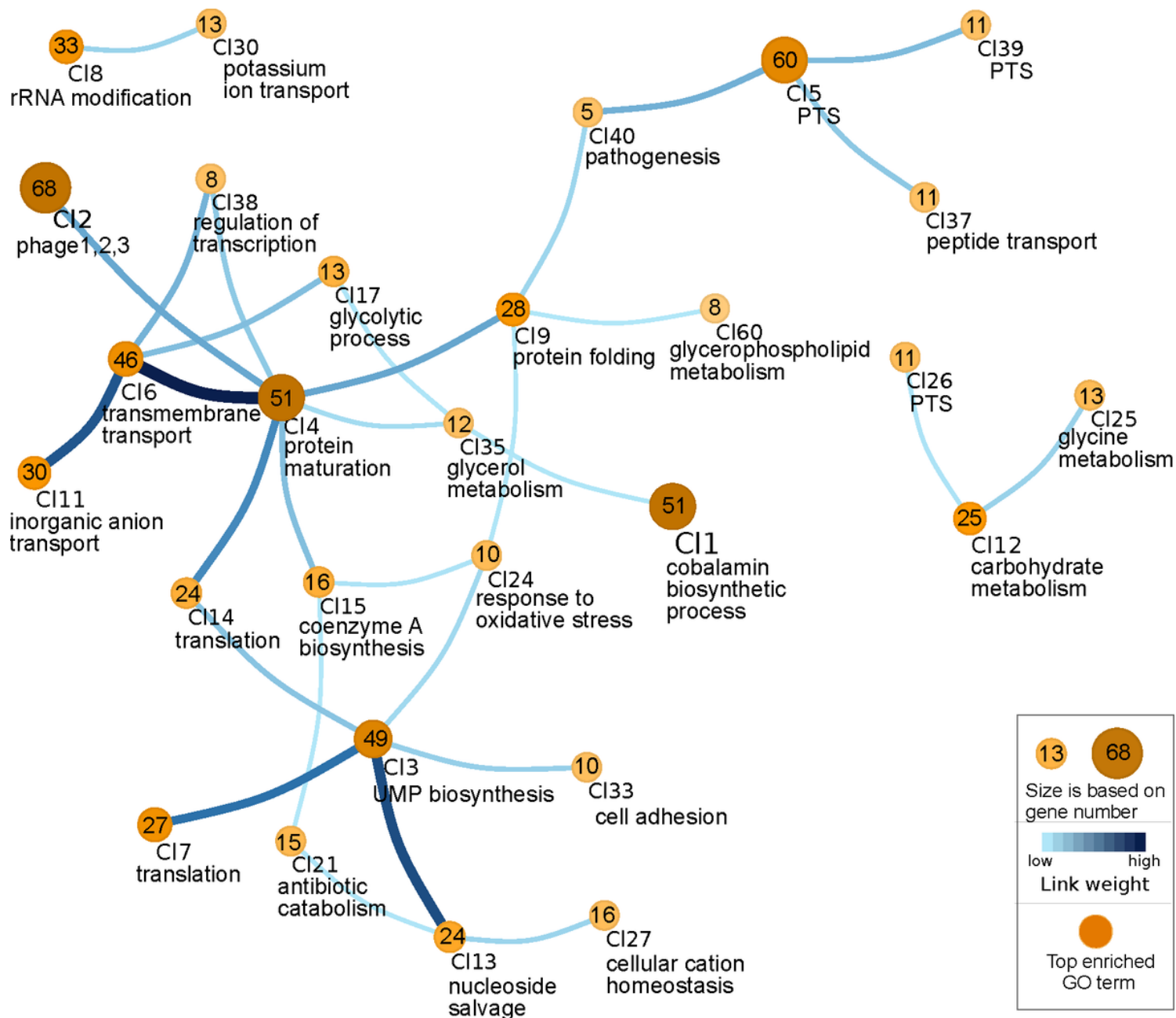


Figure 6

Visualization of clustered genes based on gene network inference in *L. monocytogenes* ScottA. Each node represents a cluster and edges represent predicted links between clusters. Number of genes within the clusters is shown in the center of the node. Below the cluster, top-scored enriched GO term is given. The used scales are described in the box. For simplification, the figure shows only the top 30 links with the highest weight, and their connected clusters. Genes within the clusters, and all links between clusters are listed in the Table S12.

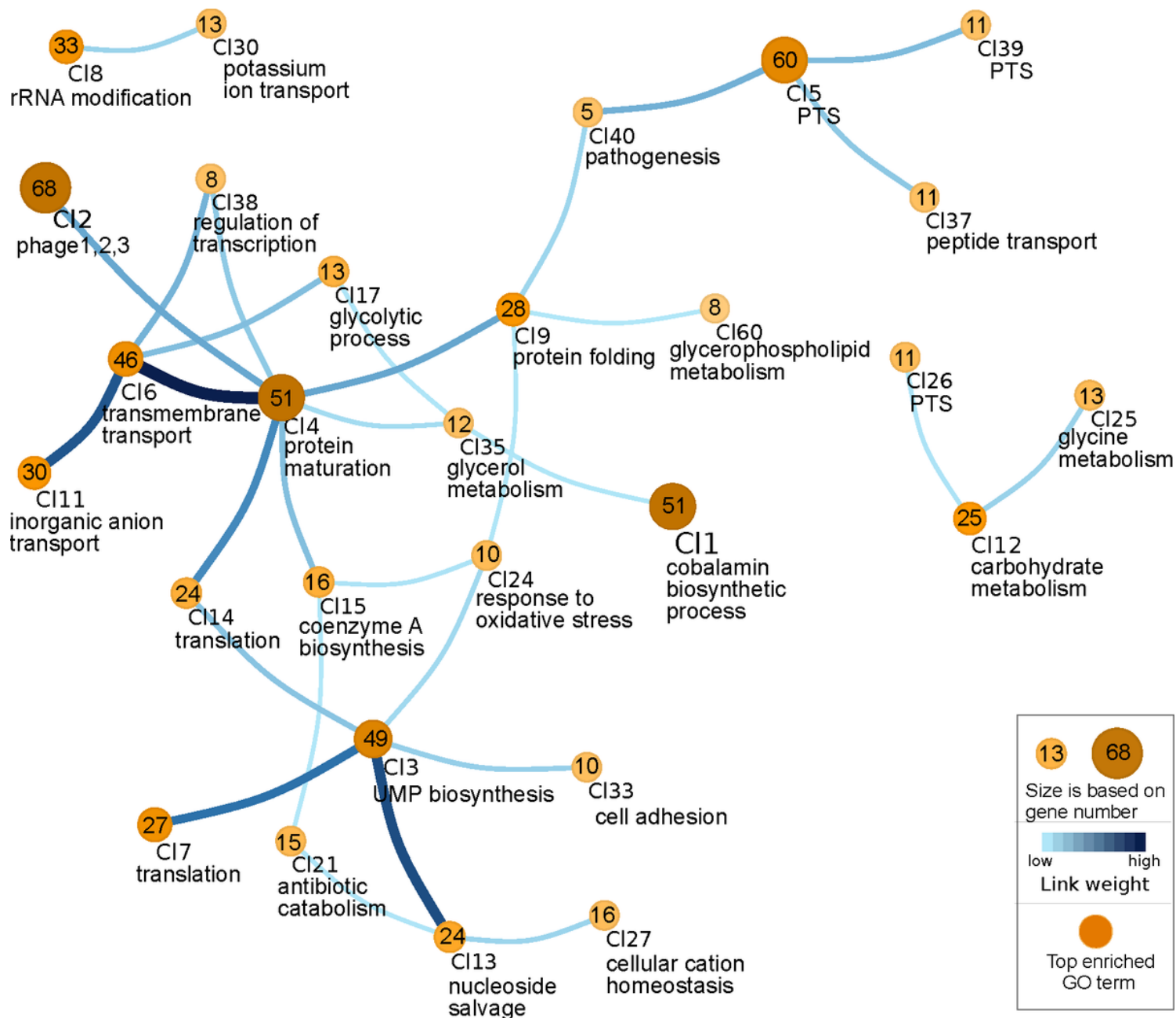


Figure 6

Visualization of clustered genes based on gene network inference in *L. monocytogenes* ScottA. Each node represents a cluster and edges represent predicted links between clusters. Number of genes within the clusters is shown in the center of the node. Below the cluster, top-scored enriched GO term is given. The used scales are described in the box. For simplification, the figure shows only the top 30 links with the highest weight, and their connected clusters. Genes within the clusters, and all links between clusters are listed in the Table S12.

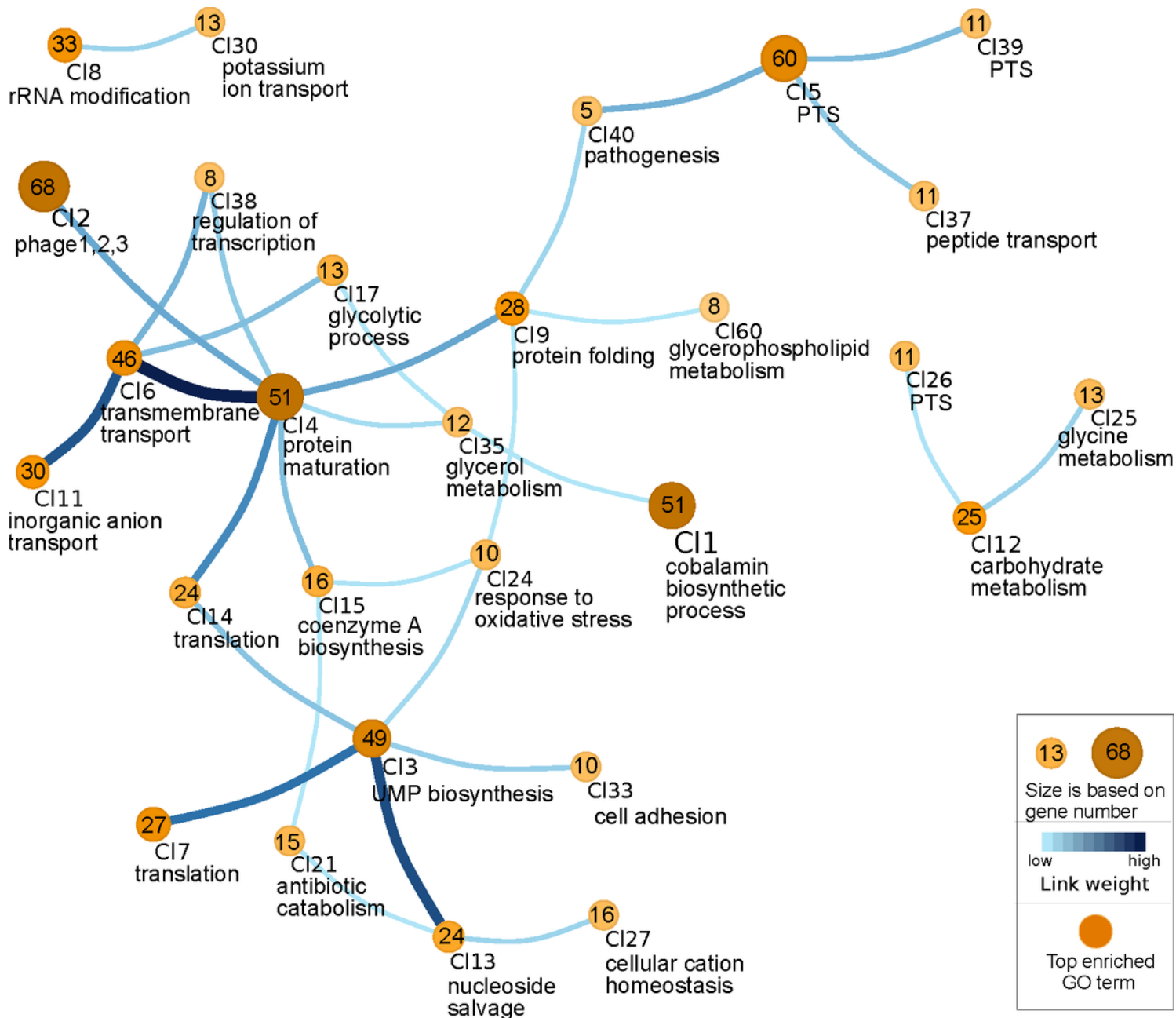


Figure 6

Visualization of clustered genes based on gene network inference in *L. monocytogenes* ScottA. Each node represents a cluster and edges represent predicted links between clusters. Number of genes within the clusters is shown in the center of the node. Below the cluster, top-scored enriched GO term is given. The used scales are described in the box. For simplification, the figure shows only the top 30 links with the highest weight, and their connected clusters. Genes within the clusters, and all links between clusters are listed in the Table S12.

recG normalized ddPCR / RNA-Seq correlation (200 MPa, 24 h)

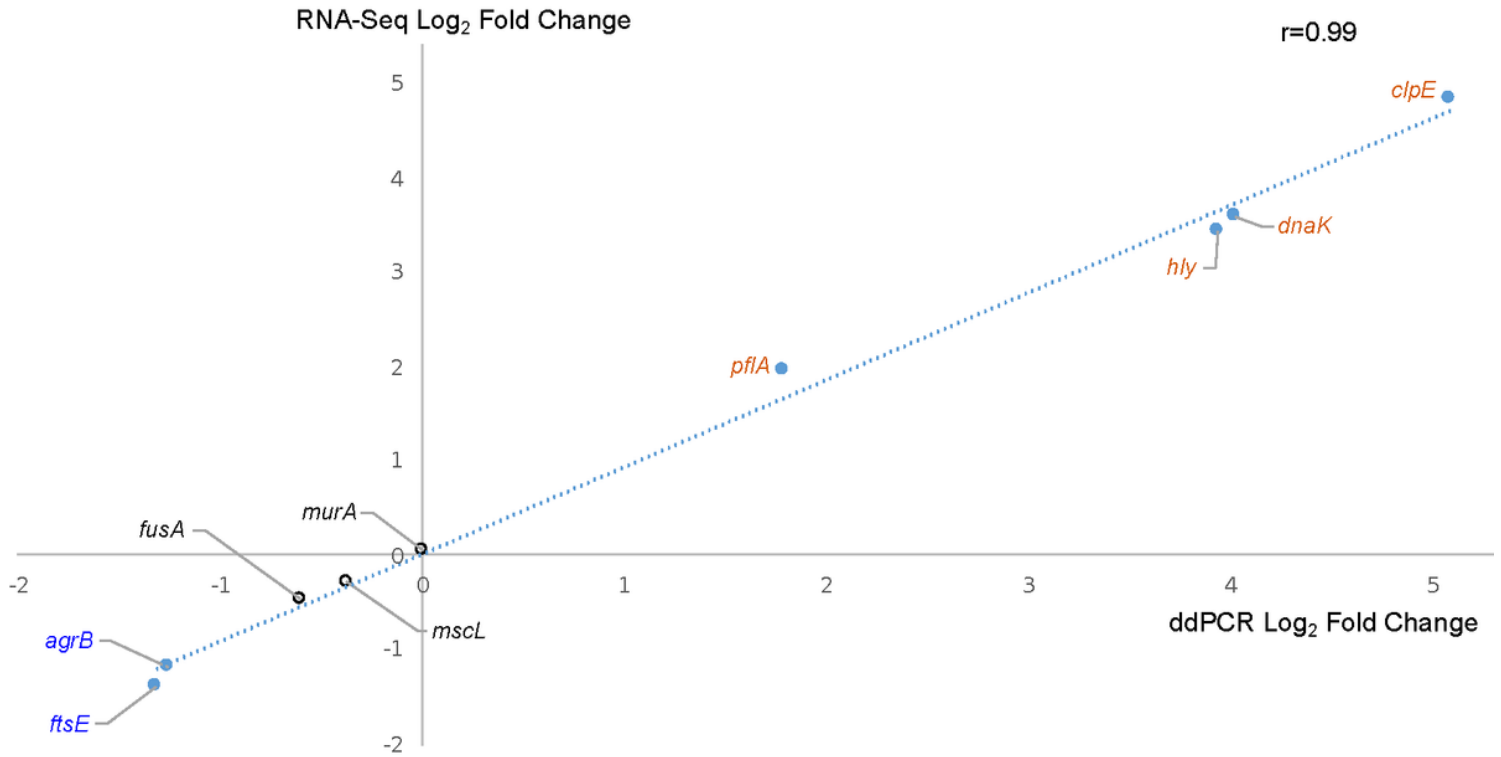


Figure 7

ddPCR / RNA-seq correlation for log₂ fold change. The figure shows log₂ fold-changes observed by ddPCR plotted against RNA-seq data for samples of ScottA obtained 24 h after treatment with 200 MPa. Transcripts levels of individual genes obtained by ddPCR were normalized to recG levels. Blue circles represent genes that were significantly differentially expressed in both ddPCR and RNA-seq results. White circles represent genes that were not significantly differentially expressed in both ddPCR and RNA-seq. The orange and blue gene names indicate significant up- and down regulation, respectively. The Pearson correlation coefficient between ddPCR and RNA-seq log₂ fold change results was 0.99 ($r=0.99$).

recG normalized ddPCR / RNA-Seq correlation (200 MPa, 24 h)

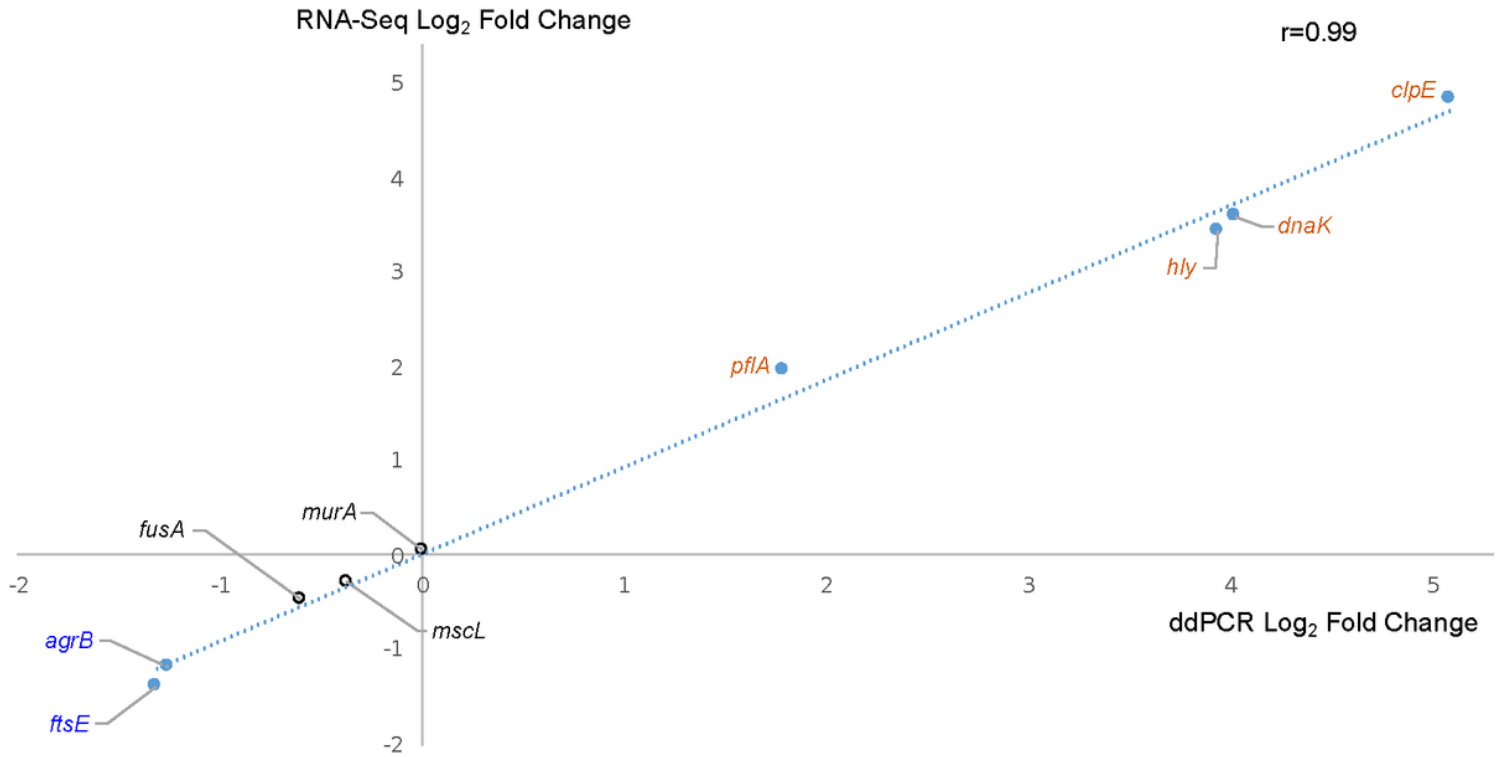


Figure 7

ddPCR / RNA-seq correlation for log₂ fold change. The figure shows log₂ fold-changes observed by ddPCR plotted against RNA-seq data for samples of ScottA obtained 24 h after treatment with 200 MPa. Transcripts levels of individual genes obtained by ddPCR were normalized to recG levels. Blue circles represent genes that were significantly differentially expressed in both ddPCR and RNA-seq results. White circles represent genes that were not significantly differentially expressed in both ddPCR and RNA-seq. The orange and blue gene names indicate significant up- and down regulation, respectively. The Pearson correlation coefficient between ddPCR and RNA-seq log₂ fold change results was 0.99 ($r=0.99$).

recG normalized ddPCR / RNA-Seq correlation (200 MPa, 24 h)

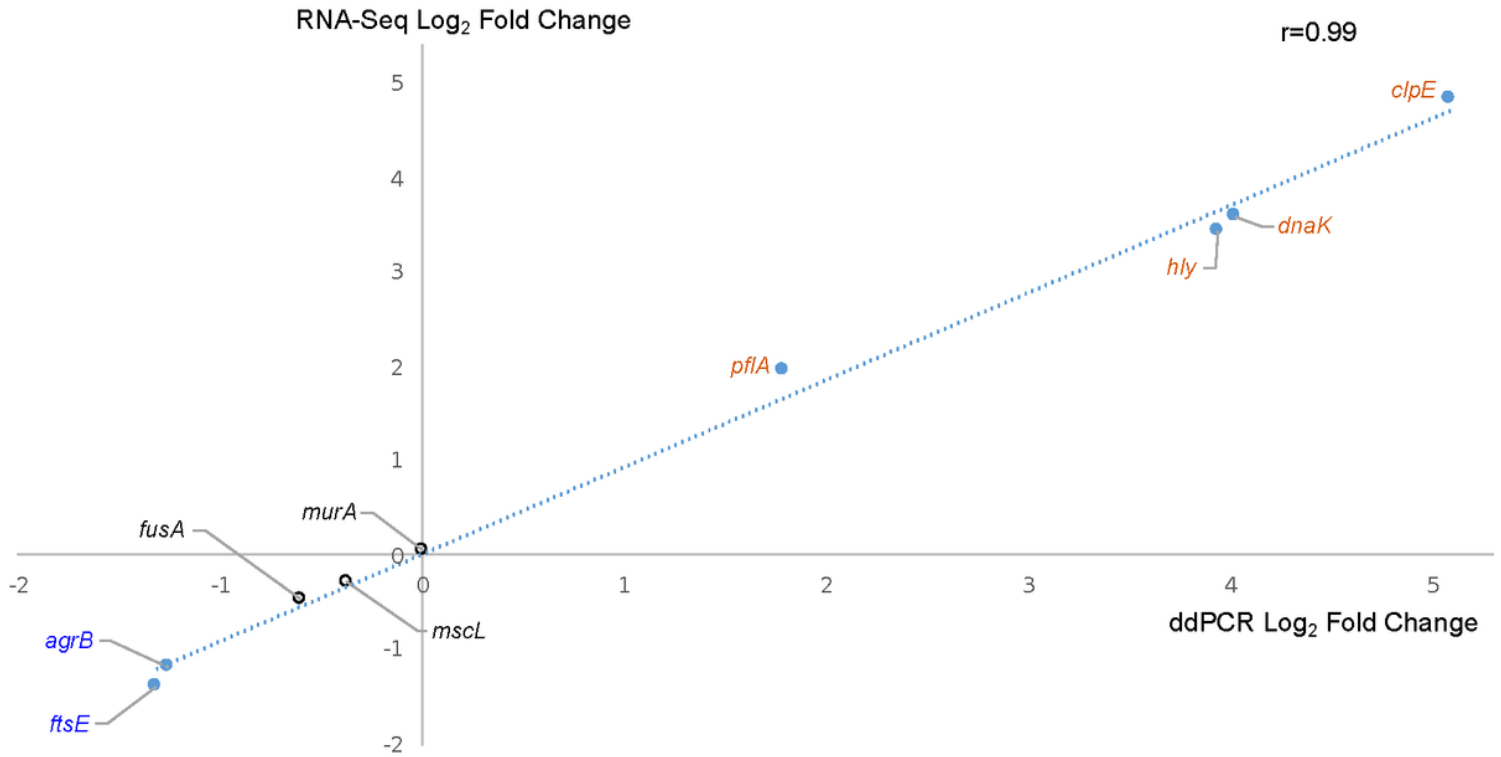


Figure 7

ddPCR / RNA-seq correlation for log₂ fold change. The figure shows log₂ fold-changes observed by ddPCR plotted against RNA-seq data for samples of ScottA obtained 24 h after treatment with 200 MPa. Transcripts levels of individual genes obtained by ddPCR were normalized to recG levels. Blue circles represent genes that were significantly differentially expressed in both ddPCR and RNA-seq results. White circles represent genes that were not significantly differentially expressed in both ddPCR and RNA-seq. The orange and blue gene names indicate significant up- and down regulation, respectively. The Pearson correlation coefficient between ddPCR and RNA-seq log₂ fold change results was 0.99 ($r=0.99$).

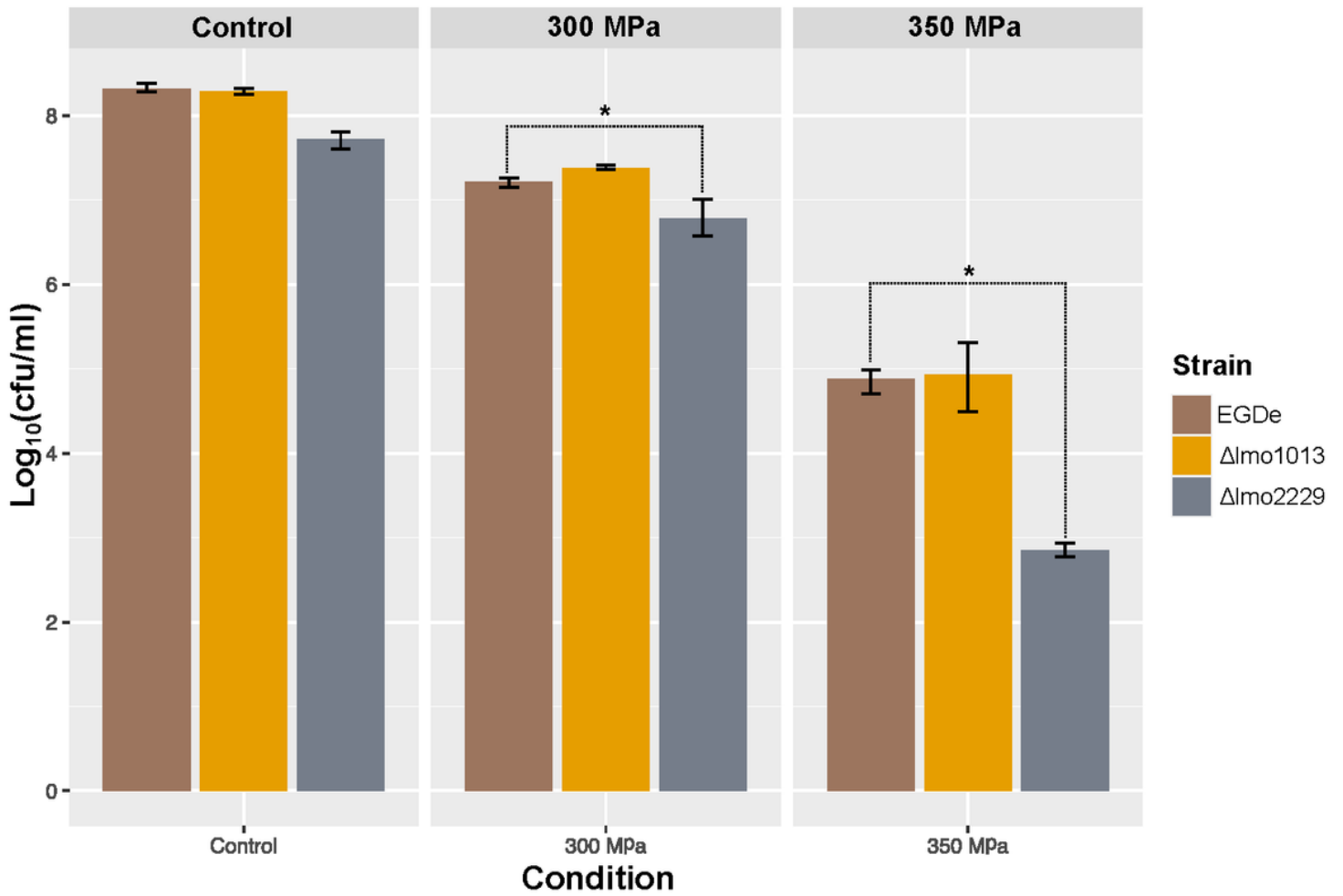


Figure 8

Effect of HPP treatments on the viability of *L. monocytogenes* EGDe, lmo1013 and lmo2229 mutants. The cells were grown at 37°C, in TSB with 0.6% YE and subjected to HPP at 300 and 350 MPa for 5 min. The results are shown for the wild-type EGDe (brown bar), Δlmo1013 (orange bar), and Δlmo2229 (gray bar). *: Student's t-test p-value < 0.05 against wild-type EGDe.

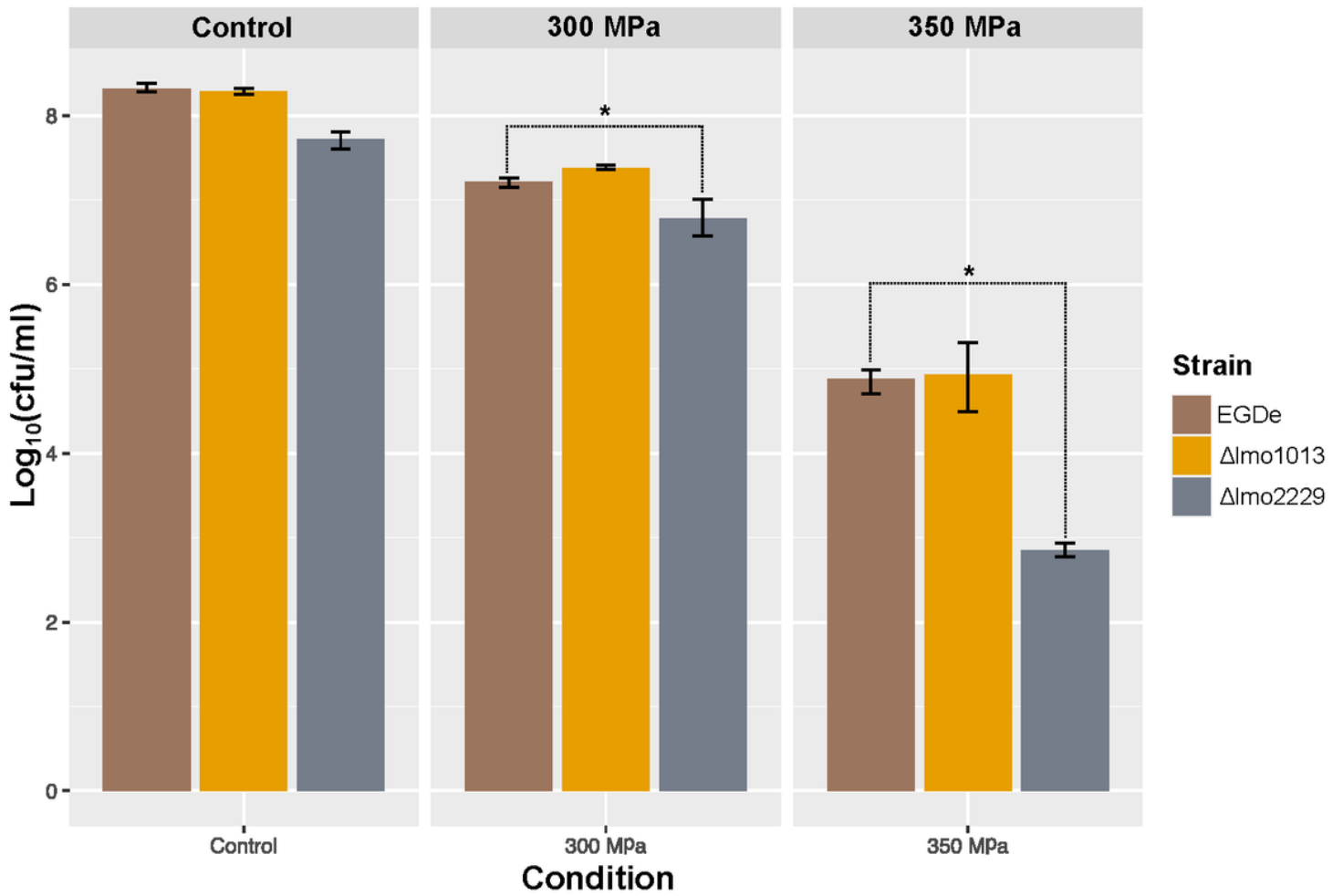


Figure 8

Effect of HPP treatments on the viability of *L. monocytogenes* EGDe, Imo1013 and Imo2229 mutants. The cells were grown at 37°C, in TSB with 0.6% YE and subjected to HPP at 300 and 350 MPa for 5 min. The results are shown for the wild-type EGDe (brown bar), ΔImo1013 (orange bar), and ΔImo2229 (gray bar). *: Student's t-test p-value < 0.05 against wild-type EGDe.

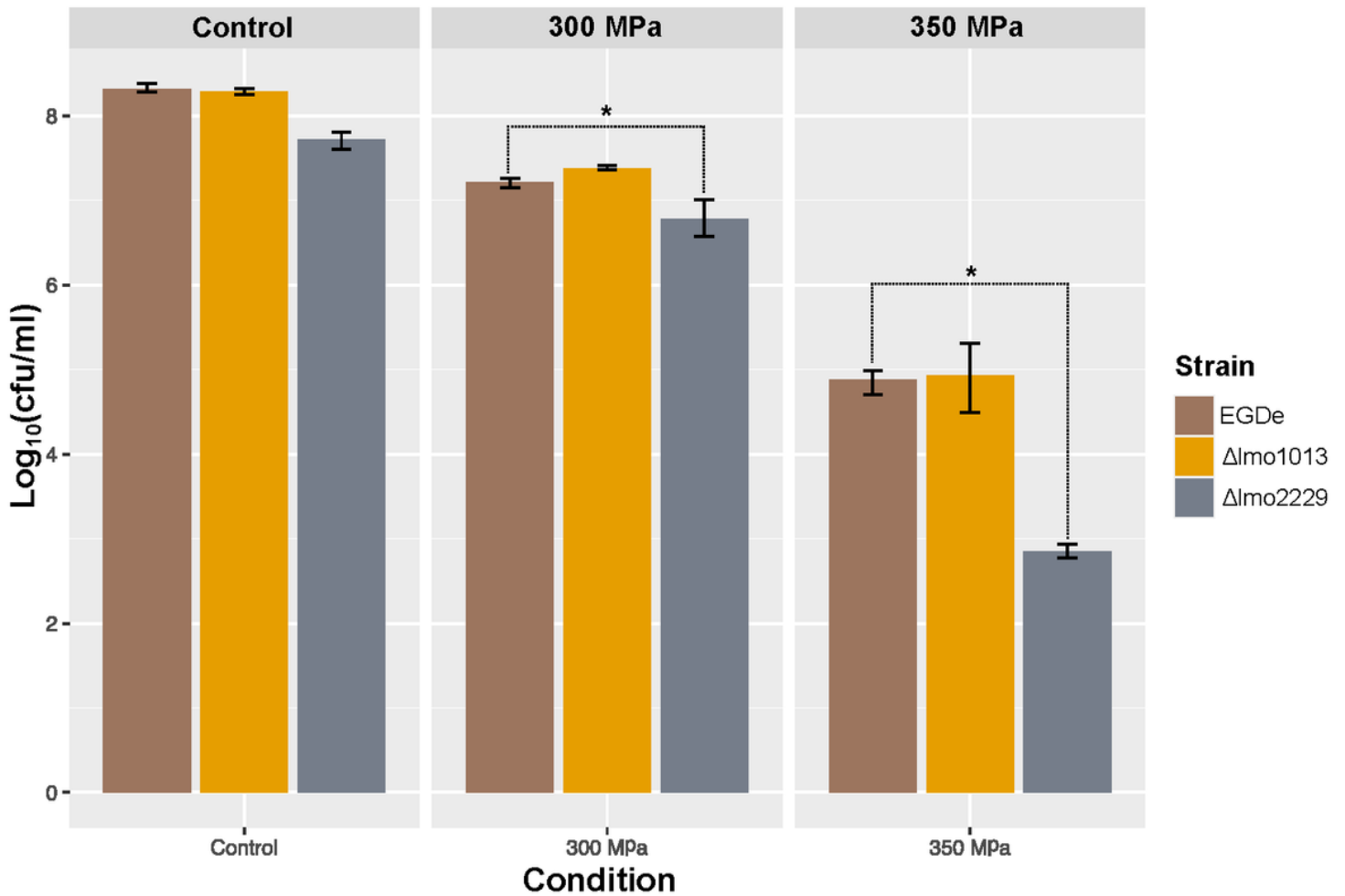


Figure 8

Effect of HPP treatments on the viability of *L. monocytogenes* EGDe, Imo1013 and Imo2229 mutants. The cells were grown at 37°C, in TSB with 0.6% YE and subjected to HPP at 300 and 350 MPa for 5 min. The results are shown for the wild-type EGDe (brown bar), ΔImo1013 (orange bar), and ΔImo2229 (gray bar). *: Student's t-test p-value < 0.05 against wild-type EGDe.

Supplementary Files

This is a list of supplementary files associated with this preprint. Click to download.

- [AdditionalFile1FigureS1.pdf](#)
- [AdditionalFile1FigureS1.pdf](#)
- [AdditionalFile1FigureS1.pdf](#)
- [AdditionalFile2FigureS2.pdf](#)
- [AdditionalFile2FigureS2.pdf](#)
- [AdditionalFile2FigureS2.pdf](#)
- [AdditionalFile3FigureS3.pdf](#)
- [AdditionalFile3FigureS3.pdf](#)

- AdditionalFile3FigureS3.pdf
- AdditionalFile4FigureS4.pdf
- AdditionalFile4FigureS4.pdf
- AdditionalFile4FigureS4.pdf
- AdditionalFile5FigureS5.pdf
- AdditionalFile5FigureS5.pdf
- AdditionalFile5FigureS5.pdf
- AdditionalFile6FigureS6.pdf
- AdditionalFile6FigureS6.pdf
- AdditionalFile6FigureS6.pdf
- AdditionalFile7FigureS7.pdf
- AdditionalFile7FigureS7.pdf
- AdditionalFile7FigureS7.pdf
- AdditionalFile8FigureS8.pdf
- AdditionalFile8FigureS8.pdf
- AdditionalFile8FigureS8.pdf
- AdditionalFile9FigureS9.pdf
- AdditionalFile9FigureS9.pdf
- AdditionalFile9FigureS9.pdf
- AdditionalFile10FigureS10.pdf
- AdditionalFile10FigureS10.pdf
- AdditionalFile10FigureS10.pdf
- AdditionalFile11FigureS11.pdf
- AdditionalFile11FigureS11.pdf
- AdditionalFile11FigureS11.pdf
- AdditionalFile12FigureS12.pdf
- AdditionalFile12FigureS12.pdf
- AdditionalFile12FigureS12.pdf
- AdditionalFile13TableS1.ods
- AdditionalFile13TableS1.ods
- AdditionalFile13TableS1.ods
- AdditionalFile14TableS2.ods
- AdditionalFile14TableS2.ods
- AdditionalFile14TableS2.ods
- AdditionalFile15TableS3.ods
- AdditionalFile15TableS3.ods
- AdditionalFile15TableS3.ods
- AdditionalFile16TableS4.ods

- AdditionalFile16TableS4.ods
- AdditionalFile16TableS4.ods
- AdditionalFile17TableS5.ods
- AdditionalFile17TableS5.ods
- AdditionalFile17TableS5.ods
- AdditionalFile18TableS6.ods
- AdditionalFile18TableS6.ods
- AdditionalFile18TableS6.ods
- AdditionalFile19TableS7.ods
- AdditionalFile19TableS7.ods
- AdditionalFile19TableS7.ods
- AdditionalFile20TableS8.ods
- AdditionalFile20TableS8.ods
- AdditionalFile20TableS8.ods
- AdditionalFile21TableS9.ods
- AdditionalFile21TableS9.ods
- AdditionalFile21TableS9.ods
- AdditionalFile22TableS10.xlsx
- AdditionalFile22TableS10.xlsx
- AdditionalFile22TableS10.xlsx
- AdditionalFile23TableS11.xls
- AdditionalFile23TableS11.xls
- AdditionalFile23TableS11.xls
- AdditionalFile24TableS12.xls
- AdditionalFile24TableS12.xls
- AdditionalFile24TableS12.xls
- AdditionalFile25TableS13.ods
- AdditionalFile25TableS13.ods
- AdditionalFile25TableS13.ods
- AdditionalFile26TableS14.ods
- AdditionalFile26TableS14.ods
- AdditionalFile26TableS14.ods
- AdditionalFile27TableS15.docx
- AdditionalFile27TableS15.docx
- AdditionalFile27TableS15.docx
- AdditionalFile28TableS16.xlsx
- AdditionalFile28TableS16.xlsx
- AdditionalFile28TableS16.xlsx

- [AdditionalFile29TableS17.xlsx](#)
- [AdditionalFile29TableS17.xlsx](#)
- [AdditionalFile29TableS17.xlsx](#)